2005

MODELING AND TESTING ULTRA-LIGHTWEIGHT THERMOFORM-STIFFENED PANELS

Prathik Navalpakkam
University of Kentucky, prathik@engr.uky.edu

ABSTRACT OF THESIS

MODELING AND TESTING ULTRA-LIGHTWEIGHT

THERMOFORM-STIFFENED PANELS

Ultra-lightweight thermoformed stiffened structures are emerging as a viable option for spacecraft applications due to their advantage over inflatable structures. Although pressurization may be used for deployment, constant pressure is not required to maintain stiffness. However, thermoformed stiffening features are often locally nonlinear in their behavior under loading.

This thesis has three aspects: 1) to understand stiffness properties of a thermoformed stiffened ultra-lightweight panel, 2) to develop finite element models using a phased-verification approach and 3) to verify panel response to dynamic loading. This thesis demonstrates that conventional static and dynamic testing principles can be applied to test ultra-lightweight thermoformed stiffened structures. Another contribution of this thesis is by evaluating the stiffness properties of different stiffener configurations. Finally, the procedure used in this thesis could be adapted in the study of similar ultra-lightweight thermoformed stiffened spacecraft structures.

KEYWORDS: Thermoformed stiffened panels, conical stiffener units, modal testing

Prathik Navalpakkam
November 2005

MODELING AND TESTING ULTRA-LIGHTWEIGHT
THERMOFORM-STIFFENED PANELS

By

Prathik Navalpakkam

_____
Director of Thesis

_____
Director of Graduate Studies

_____
Date

RULES FOR THE USE OF THESES

THESIS

Prathik Navalpakkam

The Graduate School

University of Kentucky

2005

MASTER'S THESIS RELEASE

I authorize the University of Kentucky Libraries
to reproduce this thesis in whole or in part
for purposes of research

Signed: _____

Date: _____

MODELING AND TESTING ULTRA-LIGHTWEIGHT THERMOFORM-STIFFENED PANELS

_____

THESIS

_____

A thesis submitted in partial fulfillment of the requirements for the degree of Master of Science in Mechanical Engineering at the University of Kentucky

By

Prathik Navalpakkam

Director: Dr. Suzanne W. Smith, Professor of Mechanical Engineering

Lexington, KY

2005

ACKNOWLEDGEMENTS

TABLE OF CONTENTS

Chapter One: Introduction

Chapter Two: Literature Review

Chapter Three: Static Experimentation

Chapter Four: Finite Element Modeling

Chapter Five: Dynamic Experimentation and Modeling

Chapter Six: Thesis Summary

LIST OF TABLES

LIST OF FIGURES

CHAPTER ONE

Introduction

1.1 Introduction

Man's explorations of the Solar System and search for life outside the Solar System have been significantly advanced with the recent developments in ultra-lightweight structures technology. An ever-increasing demand for greater packaging efficiencies and extremely low mass for extremely large ultra-lightweight structures used in space applications has prompted the use of structural elements consisting thin, highly flexible sheets. Today, the applications for these structures in space include lunar and planetary habitats, radio frequency (RF) reflectors and waveguides, optical and infrared (IR) imaging, solar concentrators for solar power and propulsion, sun shades, solar sails and many others. For example, Figure 1.1 shows images of the 1996 inflatable antenna experiment (IAE) deploying from shuttle STS-77and in the deployed state.
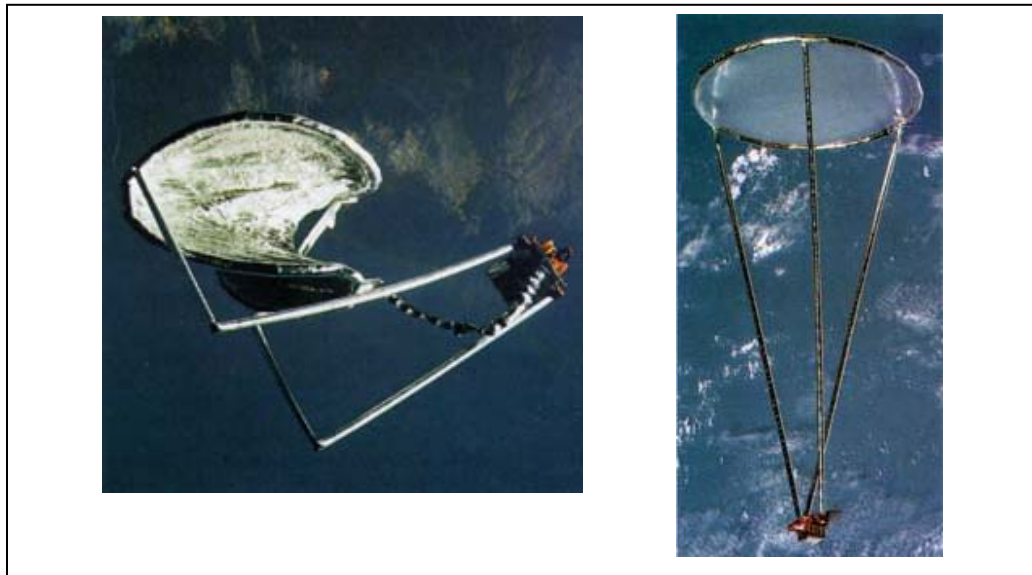
Figure 1.1: Inflatable Antenna Experiment (IAE), deploying and deployed.

The IAE structure consisted of three 28-meter long inflatable booms with a 14-meter diameter stiffened membrane reflector surface. Stiffness of the IAE reflector surface was provided by pressurization. Stiffening techniques for other large ultra-lightweight spacecraft structures is provided by pressurization, chemical rigidization or thermoforming.

Figure 1.2 presents some recent stiffened spacecraft structures. The first picture on the top left is the 15-meter wide solar array developed at ILC Dover, Inc. in support of the 2003 New Millennium Program ST4. The picture on the top right is a 7-meter rigidizing inflatable antenna prototype structure developed at L'Garde, Inc, and the picture on the bottom is an inflatable torus support structure developed at United Applied Technologies.

ST4 Solar Array, ILC Dover, Inc.

7-m rigidizing inflatable antenna prototype, L'Garde, Inc.

Inflatable torus, United Applied Technologies
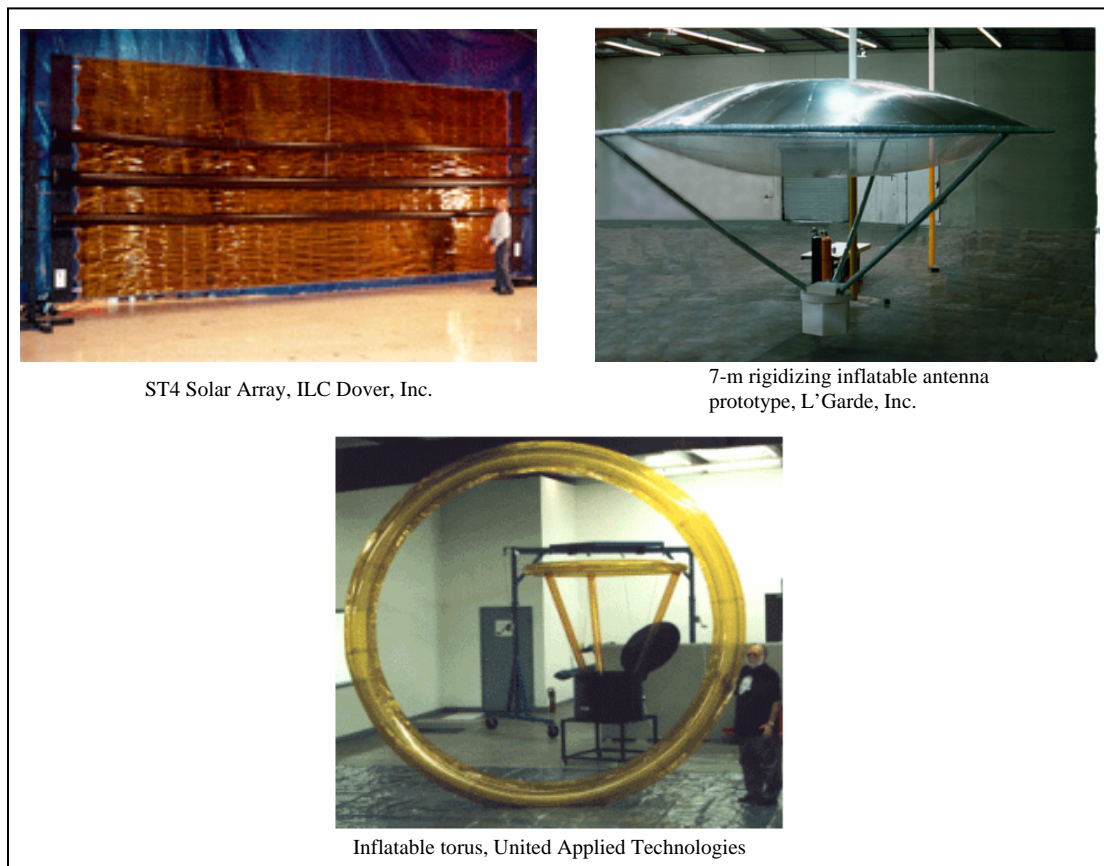
Figure 1.2: Examples of rigidized inflatable structures

Ultra-lightweight spacecraft structures have made the concept of solar sails a reality. Figure 1.3 shows an artist's concept of a solar sail using inflatable booms supporting a large surface area for propulsion. In the last five years, NASA's solar sail program has seen ground-based testing of 10-meter and 20-meter quadrants in preparation for the first on-orbit flight test.
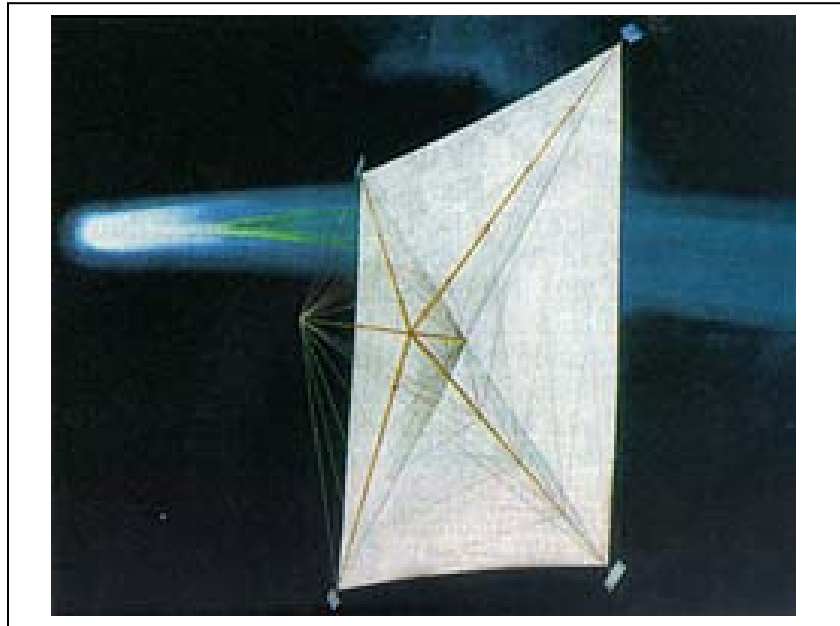
Figure 1.3: Artist's concept of a solar sail

However, even with the recent advances in materials, manufacturing, testing and other technologies for ultra-lightweight spacecraft structures, a continuing challenge is the trade-off between weight and stiffness. While pressurization and chemical rigidization have received considerable attention, thermoformed stiffening of ultra-lightweight spacecraft structures is a relatively unstudied concept. One advantage of this stiffening approach is that it replaces the need to maintain pressurization for stiffening. With thermoformed stiffeners, pressurization is used for deployment only.

1.2 Motivation

The recent development of thermoforming processes for lightweight film materials has opened the possibility of constructing ultra-lightweight panels and booms. Figure 1.4 shows an ultra-lightweight boom and ultra-lightweight panels
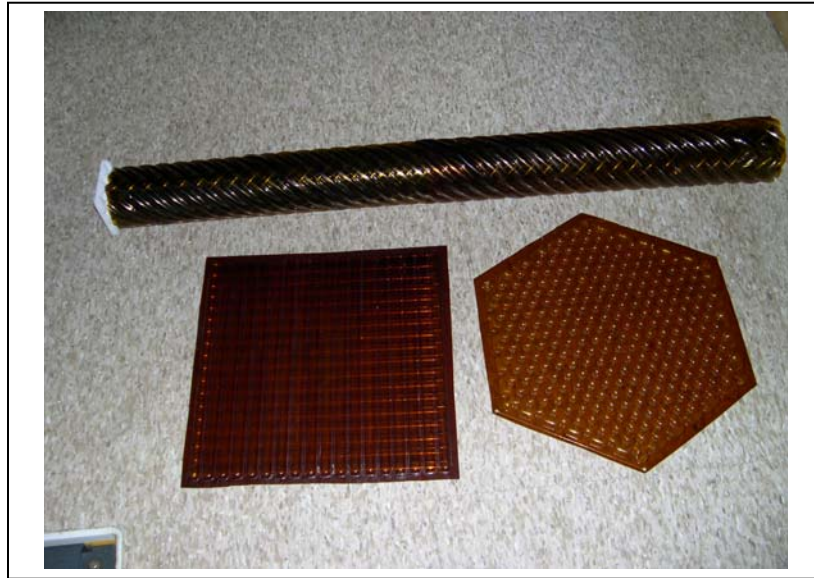
Figure 1.4: Ultra-lightweight thermoform-stiffened boom and panels

With the recent development of ultra-lightweight spacecraft structure technology and with the expense of flight experiments for technology demonstration, the need for ground-based understanding of these structures is essential. Efforts to understand the characteristics of these structures include static and dynamic testing and computer model development. The development of ultra-lightweight structures has pushed the development of new technologies such as photogrammetry and videogrammetry to measure respectively the static and dynamic behavior of large ultra-lightweight spacecraft structures. The area of ultra-lightweight thermoformed stiffened structures is new and consequently not much research has been done to date to understand their behavior in response to external static and dynamic loads.

1.3 Research Objectives and Approach

The main objective of this thesis is to develop an understanding of static and dynamic characteristics of a thermoformed stiffened panel as a representative example of this class of structures. In order to accomplish this objective, new approaches for testing are also needed for phased development and verification of finite element models. Therefore to develop a general procedure for testing and for creating finite element models using the test results is also an objective. This procedure could be adapted for application to similar panel structures or to thermoformed boom structures.

The objective is to be achieved using a phased-verification approach for testing and modeling. Static testing is first performed on individual stiffener elements, then on multiple-stiffener test sections. Based on these static test results, simple finite element models are developed and compared to the experimental results. The model is refined based on the static experiment results. Then the finite element model for the complete panel is developed. Finally, results of static and modal analysis performed on the finite element model of the complete panel are compared with the results of static and modal testing of the panel to evaluate the approach of using phased static testing for dynamic model development for thermoformed ultra-lightweight structures.

1.4 Thesis Outline

This thesis presents details of the research and results of the experimentation and analyses performed. Chapter 2 presents a review of the literature used during the course of this research work. Chapter 3 is a detailed description of the static testing and results for each of the different test articles from individual stiffener elements to the full panel. Details of developing the finite element model based on the static experiments are described in Chapter 4. Comparisons of the finite element analysis results with the static test results are also presented. Chapter 5 presents the modal testing including the test setup, procedure and results. The results of modal analysis with the finite element model,

the mode shapes and frequencies, are also presented. Chapter 6 is a summary of this thesis, with recommendations for future work also included.

CHAPTER TWO

Literature Review

2.1 Introduction

Stiffened ultra-lightweight spacecraft structures have only recently emerged as concept designs, so an extensive collection of published articles is not available. However, two sources provide wide-ranging information from materials to analysis to testing programs:

1) Gossamer Spacecraft: Membrane and Inflatable Structures Technology for Space Application referred to as "The Gossamer Handbook" published by the American Institute of Aeronautics and Astronautics (AIAA) in 2001 [1] and

2) Proceedings of the Gossamer Spacecraft Forum held annually from 2000 to present collocated with the AIAA Structures, Structural Dynamics and Materials Conference [2-4].

"The Gossamer Handbook" is a collection of contributed chapters written by experts in the field of ultra-lightweight spacecraft structures. State-of-the-art technologies of ultra-lightweight structures are presented including a wide spectrum from basic mechanics to processing issues related to membranes used in Gossamer structures. It also provides valuable information about testing and modeling of these unique, flexible structures. The handbook includes contributions of major research organizations such as the Air Force Research Laboratory (AFRL), Jet Propulsion Laboratory (JPL) and others and from primary industrial participants such as ILC Dover, SRS Technologies, L'Garde and United Applied Technologies. This book provides a wealth of knowledge in the area of ultra-lightweight spacecraft structures with a new edition currently underway.

The Gossamer Spacecraft Forum is a conference for university, industry and national laboratory researchers to exchange information on recent advances in Gossamer spacecraft technologies. Each year, the proceedings are a compilation of about 50 to 60

papers on topics such as spacecraft structures, membrane rigidization concepts, analytical dynamic modeling of inflatable structures, stability of inflatable structures and others. The seventh forum is scheduled for May 1-4, 2006 in Newport, RI.

The remainder of this chapter presents a review of references that were used during this thesis research. It also highlights the various activities performed in field testing and modeling of ultra-lightweight space structures.

2.2 Ultra-Lightweight Spacecraft Structures

Ultra-lightweight spacecraft structures include inflatables, solar sails, sun shields, and stiffened ultra-lightweight panels, among others. Companies involved in testing and manufacturing of these structures include ILC Dover, Inc., L'Garde, United Applied Technologies, SRS Technologies and others. ILC Dover, Inc. [5] has built and tested several inflatable space structures including inflatable antennas and inflatable solar arrays. Several rigidization techniques have evolved over the years to provide stiffness to these structures. Some of the stiffening features include pressurization, rigidization and thermoforming. L'Garde [6] developed a 7-meter rigidizing inflatable antenna prototype structure. United Applied Technologies [7] have developed preformed inflatable torus structures and self-rigidizing thin film structures, curved thin film concentrators and others. SRS Technologies [8] developed a 5-meter diameter thin film antenna prototype, 10-meter and 20-meter solar sail test articles, sun shields and others.

Inflatable torus structures are important to spacecraft systems providing structural support to antennas such as the IAE and to optical systems such as thin membrane reflectors or solar collectors. The dynamic behavior of the torus structure is of primary interest in the design of these systems [9-13].

2.3 Modal Testing of Ultra-Lightweight Inflatable Structures

This main focus in this thesis was to test and model an ultra-lightweight panel structure with thermally-formed stiffener units. Standard modal testing principles were used to test the panel structure as described in classic references by Ewins [14] and McConnell [15].

Griffith performed experimental and analytical modal analysis of an inflated thin film torus and demonstrated that conventional modal testing principles could be applied to ultra-lightweight inflatable structures. Griffith used a modified impact hammer for exciting the torus to prevent local deformations [16].

Lassiter conducted modal tests on torus-supported solar concentrators. He demonstrated that inflatable structures are sensitive to extraneous disturbance and hence caution is required while performing dynamic tests on these structures. Also, the selection of proper boundary conditions is crucial in testing these structures as they need supports with extremely low stiffness [17].

Lassiter and Slade performed modal tests on inflatable solar concentrators using a non-contacting laser vibrometer measurement system, measuring frequency response functions. They compared mode shapes and frequencies among thermal vacuum tests for different inflation pressures. They highlighted the need for performing in-vacuum tests of inflatable structures [18].

Ruggiero and Inman evaluated the use of smart materials for vibration testing and control of a 1.8-meter diameter inflated torus structures with no thermoformed stiffeners. They advanced the idea that smart materials demonstrated flexibility and had high electromechanical coupling, and so concluded that smart materials were ideal for applications involving dynamics and control of inflatable structures [19].

Inman and Sodano performed modal tests on a scaled inflatable macro-fiber composite torus without thermoformed stiffeners. They highlighted the advantages of using multiple sensors for controlling inflatable structures [20].

Song performed modal tests on a self-supporting thin-film torus structure with thermoformed domed hexagon pattern stiffeners using a speaker to provide acoustic excitation. The displacement response was measured using a laser displacement sensor. Together, these demonstrated that a non-contacting excitation and measurement approach is suitable and effective for modal testing of thermoformed stiffened structures. Figure 2.2 shows a picture of modal testing on the stiffened torus structure [21].
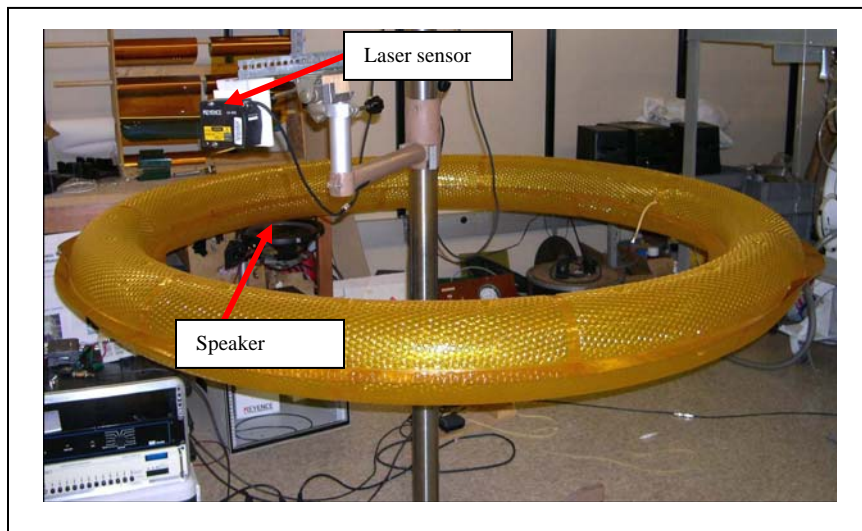
Figure 2.1: Inflatable torus structure tested by Song [21]

These more traditional modal testing approaches serve as a viable alternative for stiffened ultra-lightweight structures, as opposed to unstiffened ultra-lightweight structures which require alternative and specially developed measurement technologies.

2.4 Emerging Techniques for Testing Ultra-Lightweight Structures

Photogrammetry and videogrammetry are among other testing methods used to test ultra-lightweight structures. Black applied photogrammetry and videogrammetry methods for static and dynamic characterization of Gossamer structures [22]. Figure 2.1 shows the test setup that was used for dynamic characterization, allowing comparison between results from laser vibrometry and videogrammetry.
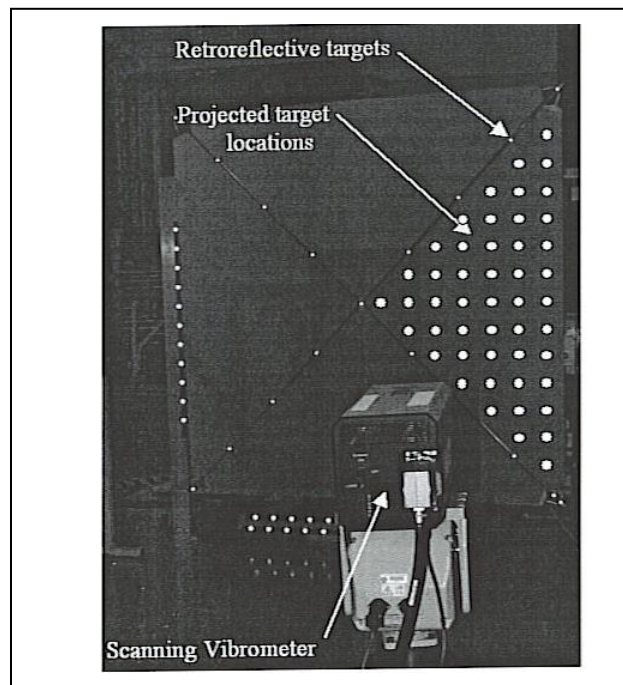
Figure 2.2: Test setup for dynamic characterization using photogrammetry [22]

Thota applied the principles of photogrammetry and videogrammetry to measure in-plane displacements of thin-film structures using etched surface patterns. He demonstrated that the etching pattern does not have significant effect on the dynamic in-plane displacement [23].

2.5 Modeling Ultra-Lightweight and Inflatable Structures

One of the main objectives of this thesis was to develop a finite element model of the ultra-lightweight panel to accurately represent its properties. The size of the model was a concern, with so many stiffening elements in the design. Lore applied Automated Multi-Level Sub Structuring (AMLS), widely used in the automotive industry for modal analysis of extremely large models, to evaluate its use for designing thermoformed stiffened spacecraft. Lore found that using detailed models of individual stiffening elements was computationally prohibitive because the models created had too many degrees of freedom (dofs) for a solution to be computed. Even simplified models of thermoformed stiffeners produced models of the thermoformed stiffened torus with more than one million dofs [24].

A study was conducted by the author of this thesis to understand the detail required in a thermoformed stiffener model in a large structure model. Note that a finely detailed mesh of the stiffeners of the 2-meter torus in Figure 2.2 was estimated to have 8.9 million dofs. The simplest accurate model of the stiffeners would result in a torus model with approximately 2.9 million dofs. Further reduction of the number of dofs in the stiffener model could lead to loss of accuracy. The size of the stiffener relative to the size of the structure is an important factor in the ability to simplify the model of the stiffener element. As the size of the stiffener becomes smaller, the model can become simpler without losing the ability to accurately represent the dynamic response [19].

Palisoc and Huang developed a geometric nonlinear finite element solver, Finite Element Analysis of Inflatable Membranes (FAIM) with nonlinear material capability. This provided an integrated set of tools for analysis and design of inflatable antennas [25].

2.6 Modeling Inflatable Booms

Inflatable booms are important for providing support to solar arrays, solar sails, reflectors and other ultra-lightweight spacecraft structures. Some of the efforts to understand the behavior of these structures to both static and dynamic loads are presented in this section.

Herbeck and Eiden computed the stability behavior of inflatable boom structures used for solar sails applying conventional finite element methods. They computed the buckling limits of the structure using linear and nonlinear models [26].

Lou and Fang developed a finite element model of an inflatable boom and performed static analysis. They compared the results of this analysis with their experimental results for different internal pressures [27].

Virgin developed finite element models of slender inflatable booms used for solar sails and verified the models with experimental results. Virgin analyzed specific structural aspects of the solar sail inflatable booms [28].

2.7 Summary

Various approaches to testing and modeling ultra-lightweight structures presented in this chapter provided insight and background knowledge to this thesis. The modal testing approach using a modified impact hammer was adapted and conventional testing principles highlighted in some references mentioned above have been applied in this thesis. Appropriate testing conditions have been applied to perform near free-free modal testing based on the lessons learned from reviewing the reference materials.

CHAPTER THREE

Static Experimentation

3.1 Introduction

This chapter introduces different panel types and develops classifications. It presents details of the panel geometry and construction that determine their overall properties along with static and dynamic response characteristics. Static experiments performed to understand the behavior of panels are also presented in this chapter, with details of the experimental setups and procedures. The progression of deformation is quantitatively described as observed during panel loading and unloading. Results of the tests are discussed.

3.2 Panel Construction and Geometric Details

The ultra-lightweight stiffened panels considered in this thesis are comprised of a number of layers of thermally-formed Kapton as shown in Figure 3.1. The thermoforming process induces permanent deformation in the Kapton sheet which acts as a stiffening substructure in the panel. For this thesis, the focus panel is hexagonal, as seen on the right in Figure 3.1, and has conical stiffeners (stiffening units) equally spaced in a hexagonal honeycomb fashion.

The number of layers depends on the application which in turn defines requirements including physical strength, weight, size constraints etc. A one-layer panel has one layer; a two-layer panel has two layers bonded mirror image (Figure 3.2). The thickness of the assembled panel thus depends on the height of the cones. The area of the panel depends on the cone base radius and the spacing between them. The size and geometry of the cones varies for each panel depending on the desired stiffness and buckling stability.
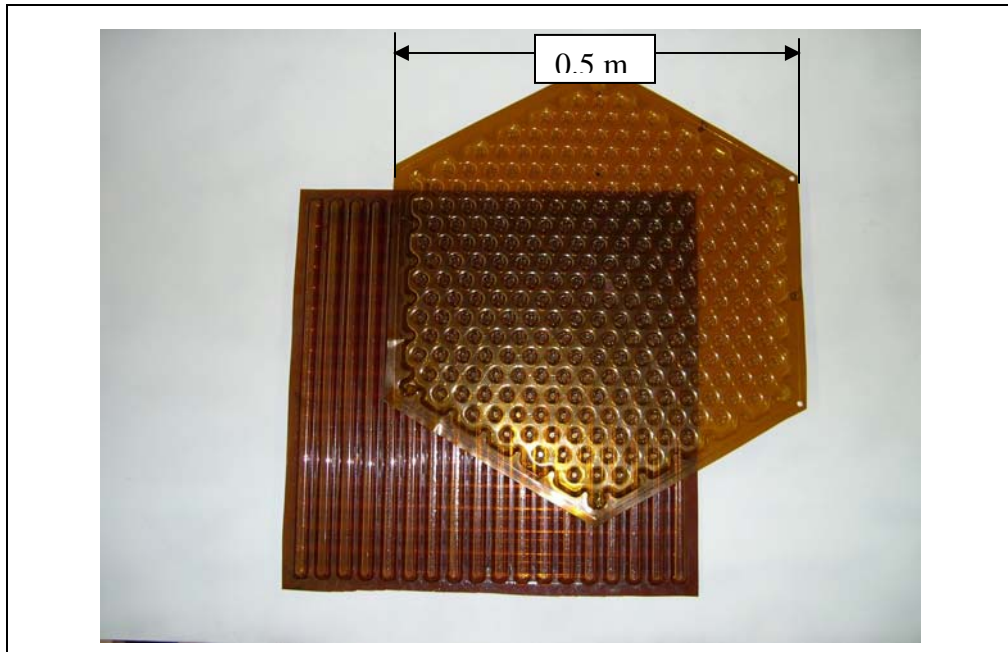
Figure 3.1: Examples of thermally-formed Kapton panels representative of ultra-lightweight stiffened spacecraft structures

One-layer panel
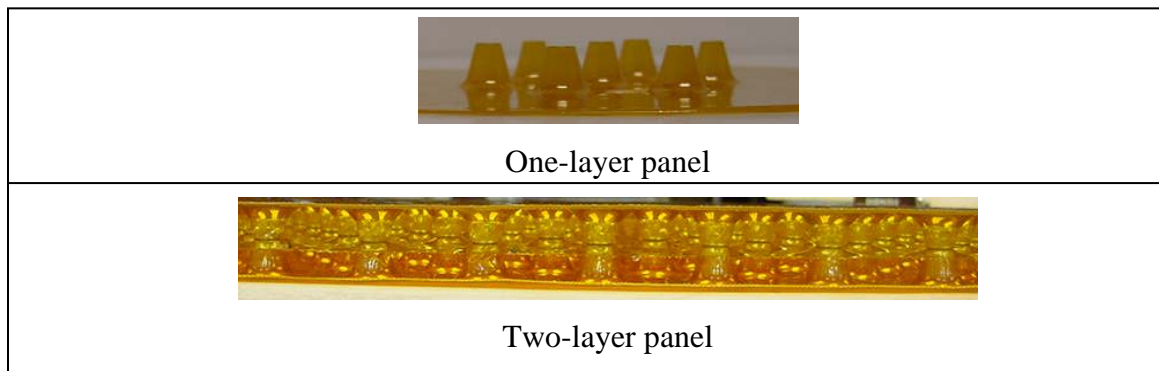
Two-layer panel

Figure 3.2: One-layer and two-layer panels

Individual stiffening units of the panel are conical in shape as seen in Figure 3.2. Circular cones and hexagonal cones are considered in this thesis, but other cross-section geometries are possible. The circular cones have a varying cross-section radius from top to bottom. Thermoformed straight-sided stiffeners are also possible. The conical configuration contributes significantly to the behavior of these units when subjected to loads.

The two-layer panel tested for this thesis consists of the two cones that are bonded to each other (as presented in Figure 3.3) at the contact surface to avoid relative lateral movement while being loaded.
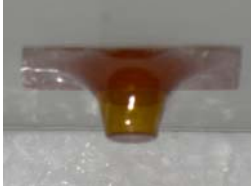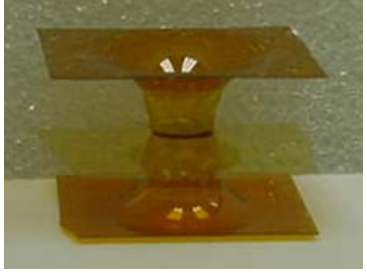
		Two-layer sample
Top cone		
Bottom cone		

Figure 3.3: Top cone and bottom cone of two-layer panel

Each panel is characterized by several dimensional parameters which are controlled during the manufacturing process. These parameters are critical to their performance when subjected to loading. The parameters are illustrated in Figure 3.4 in which

t is the thickness of the Kapton sheet,

T is the assembled panel thickness,

r is the smallest radius of the cone,

R is the largest radius of the cone,

h is the cone height, and

d is the center-to-center distance between adjacent cones in a layer.
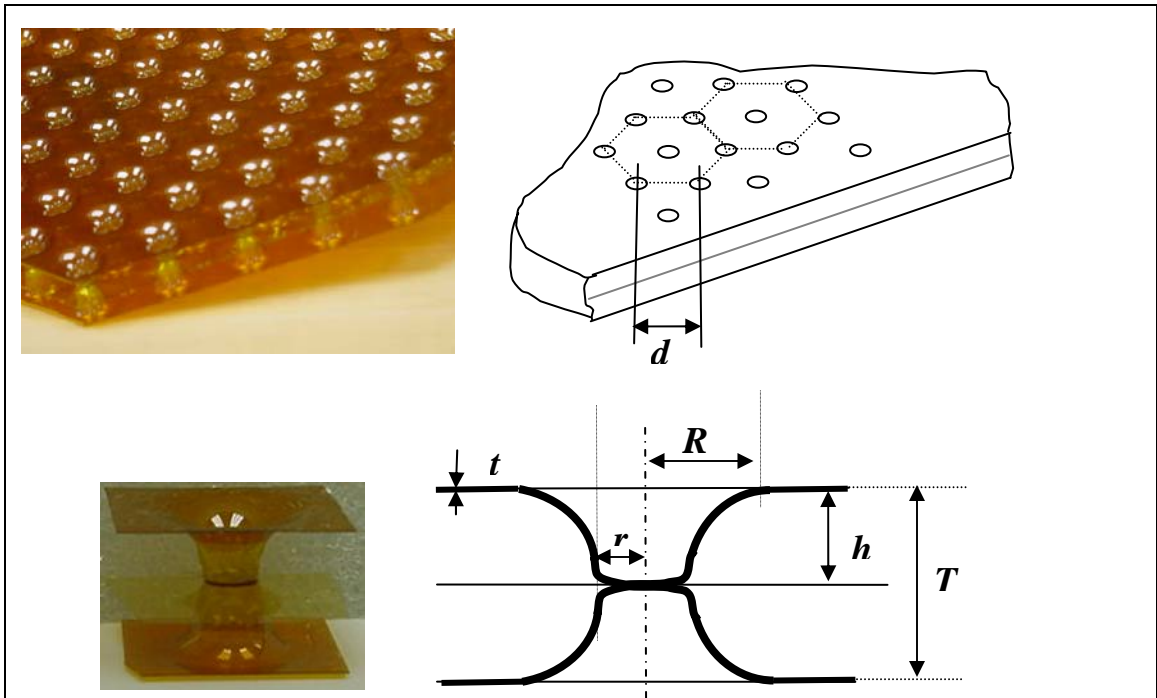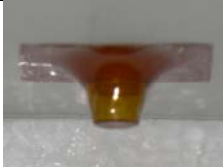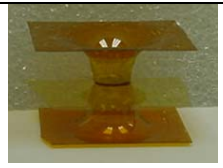
Figure 3.4: Dimensional parameters of a panel

3.3 Static Experiments of Single-Unit Stiffeners

A series of static experiments were conducted on stiffening units and on panels of varying configurations. These experiments were aimed mainly at understanding the stiffness characteristics of the stiffener units and of the assembled panels. Table 3.1 presents the different samples that were tested to develop an understanding of unit conical stiffener behavior.

Table 3.1: Unit stiffener samples and four-unit sample tested

Sample designation	Configuration	Dimensions	Picture
Sample A1	One-unit, one-layer panel, top cone	r= 3.17mm h=7.93mm R = 15.87mm	
Sample A2	One-unit, one-layer panel, bottom cone	r=3.17mm h=7.93mm R=15.87mm	
Sample B	One-unit, two-layer panel	T=15.87mm	
Sample C	Four-unit, two-layer panel	d=25.4mm	

The experimental setup for one-unit and four-unit samples consists of a sensitive weighing scale (Ohaus model EP4102 C) and a precision movable platform (Newport model 340RC) used to displace the samples. As seen in Figure 3.5, the sample is mounted securely to the platform and then lowered until it is just in contact with the scale. The scale is then set to zero and the test is started from this point.
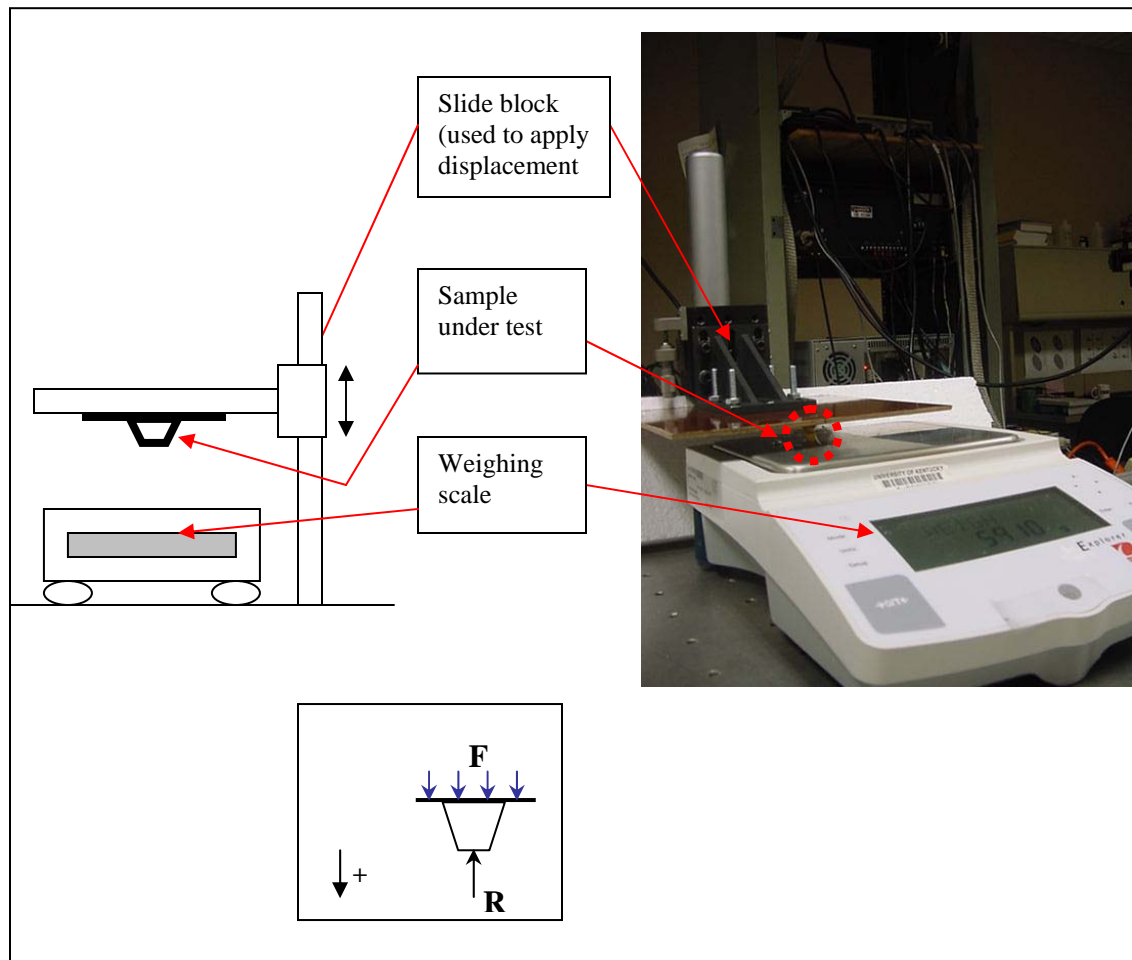
Figure 3.5: Experimental schematic and setup for static test of panel units.

The loading cycle consisted of a series of precise displacements, first increasing the vertical force on the sample and then decreasing it. The free body diagram is also presented in Figure 3.5 with the sign convention for displacement. Displacements in steps of 0.05mm were used. The corresponding reaction force displayed on the scale was recorded. The load was then slowly released by reversing the displacement sequence by raising the slide block in increments of 0.05mm. Again, the corresponding reaction force was recorded for each step. The force-displacement results were consistent. The results of this test are presented in Section 3.4 and the test data is presented in Appendix 1.

Figure 3.6 shows the load-displacement plot for a single loading cycle of the one-unit, one-layer top cone, sample A1. The vertical axis is the force in Newtons. The horizontal axis is the corresponding displacement in mm. The slope of the curve is approximately 3 N/mm. The loading and unloading sequences are not identical, forming a hysteresis loop. Both the loading and unloading cycles show a slight stiffening trend (an increasing slope with increasing displacement).
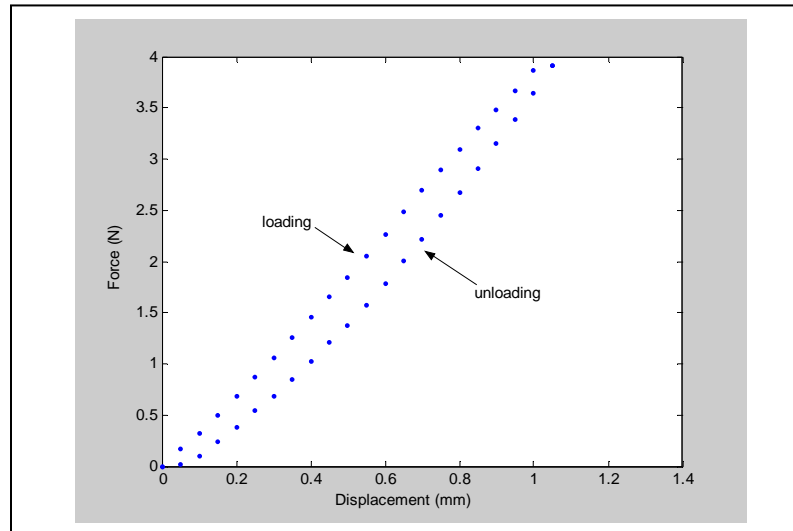
Figure 3.6: Force-displacement plot for Sample A1

The load-displacement plot for a single loading cycle of the one-unit, one-layer bottom cone, sample A2 is presented in Figure 3.7. It should be noted that sample A1 and A2 have the same height. However, in sample A1, the conical area is thinner for greater sections of the cone compared to sample A2. Here, the loading and unloading results are

similar to those of sample A1, also forming a hysteresis loop. The slope of the curve is approximately 5 N/mm and is about 66% stiffer than the sample A1. Both loading and unloading cycles show a slight stiffening trend, although less than that seen in sample A1.
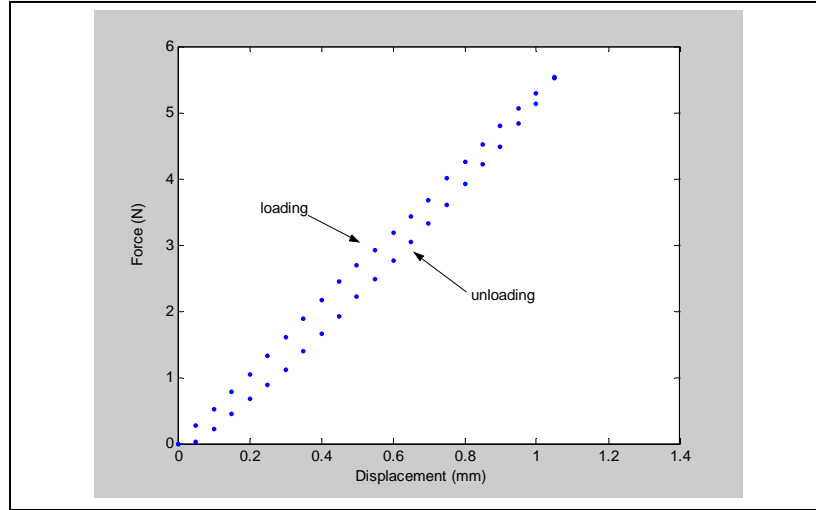
Figure 3.7: Force-displacement plot for Sample A2

Following the static test on samples A1 and A2, the one-unit, two-layer sample B was tested. The same test procedure and test setup as for samples A1 ad A2 were used. Two sample B units were tested. Results for both are included in Appendix 1. Force-displacement results for one sample are presented in Figure 3.8. This loading and unloading sequence was repeated three times. Here, the force-displacement plots indicate that the slope increases significantly beyond a certain load. For small loads, the deformation of the top cone appeared to be more prominent. With higher loads, the top cone had deformed up to a certain point beyond which deformation of the bottom cone was noticed. The slope of the lower portion of this plot is approximately 1.5 N/mm and that of the steeper portion of this plot is approximately 3 N/mm compared to the calculated combined slope of approximately 2 N/mm with top cone and bottom cone modeled as springs in series.
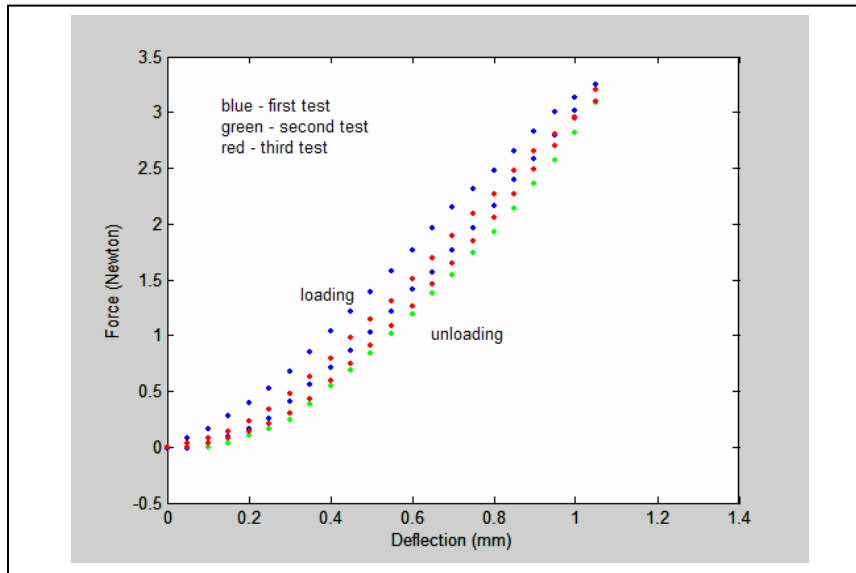
Figure 3.8: Force-displacement plot for sample B1

Figure 3.9 illustrates the progression of local deformations of the two-layer, one-unit panel (Sample B) unit as observed during the loading cycle. It is described in six-steps. Step 1 indicates the sample condition at the time of applying the loads. As the load is applied gradually, the top cone of the sample begins to twist as indicated in step 2. The top cone twists up to a particular point beyond which further application of load causes the bottom cone to twist. This process is initiated by signs of buckling of the top cone as can be seen in step 3. Beyond this point, the bottom cone begins to deform as in step 4. Further loading causes the two cones to buckle. This sequence of progression is observed for every load cycle of the samples. The twisting of the cones was more prominent to the naked eye in the two-layer, one-unit samples.
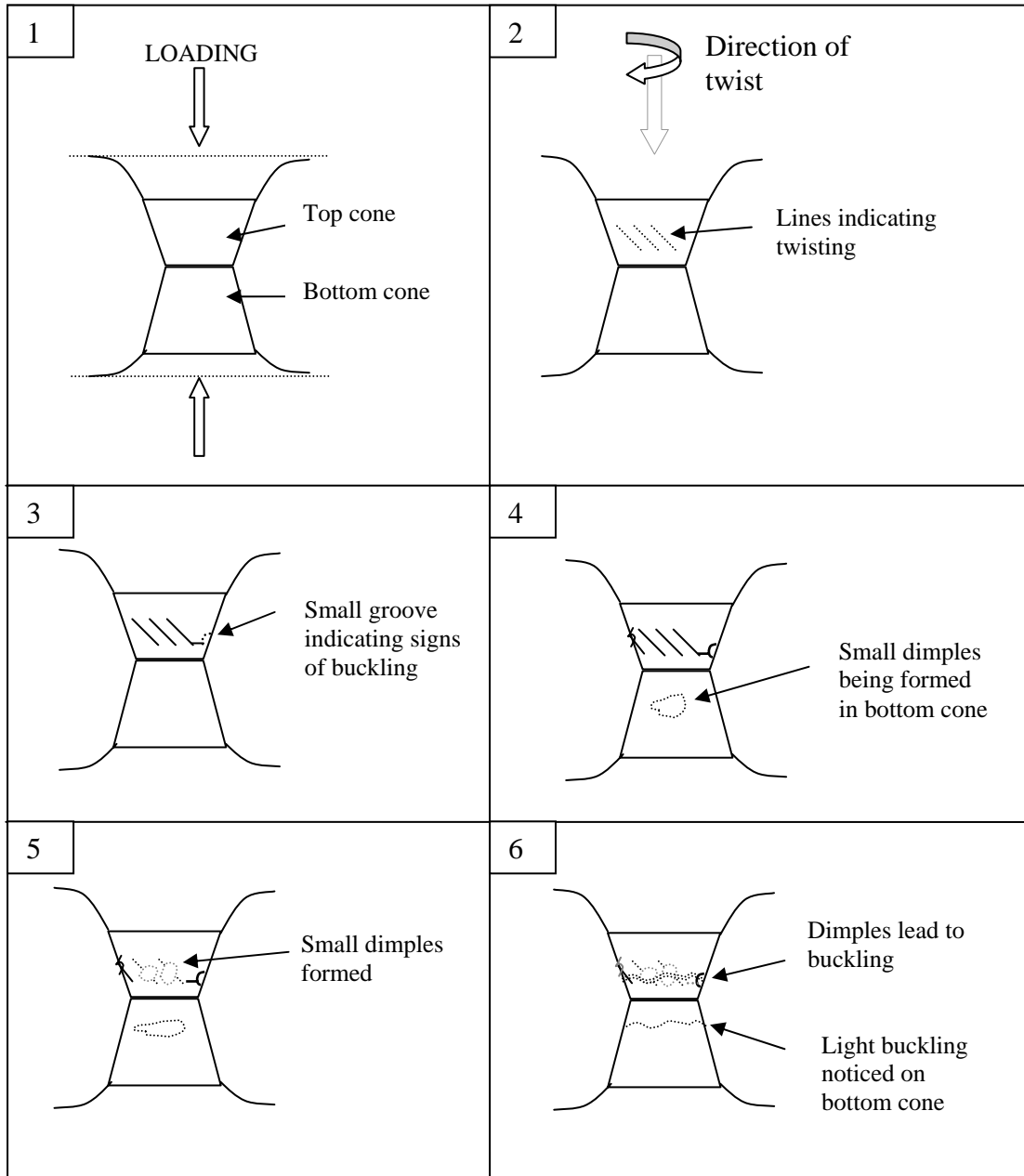
Figure 3.9: Schematic representation of progression of deformation for two-layer, one-unit sample under loading

Figure 3.10 presents the force-displacement results for the four-unit-two-layer panel (Sample C). The stiffness of the lower portion of this plot is approximately 2 N/mm and the steeper portion of this plot is approximately 10 N/mm compared with the calculated slope of 7.5 N/mm with four two-layer-one-unit samples in parallel. The transition point of the curve occurs approximately at 0.25 N. It can be seen that the sharper bilinear property of the individual units as seen in Figure 3.8 is smoothed for the four-unit-two-layer sample where four stiffener units are combined together in parallel. The force-displacement plot of the four-unit-two-layer sample in Figure 3.10 shows a smoother transition from the lower less-stiff slope to the steeper portion compared to the one-unit-two-layer stiffeners in which case the transition can be approximated as a bilinear stiffness. The approximate calculated stiffness of four series springs in parallel is 7.5 N/mm based on the static test experiments on samples A1 and A2.
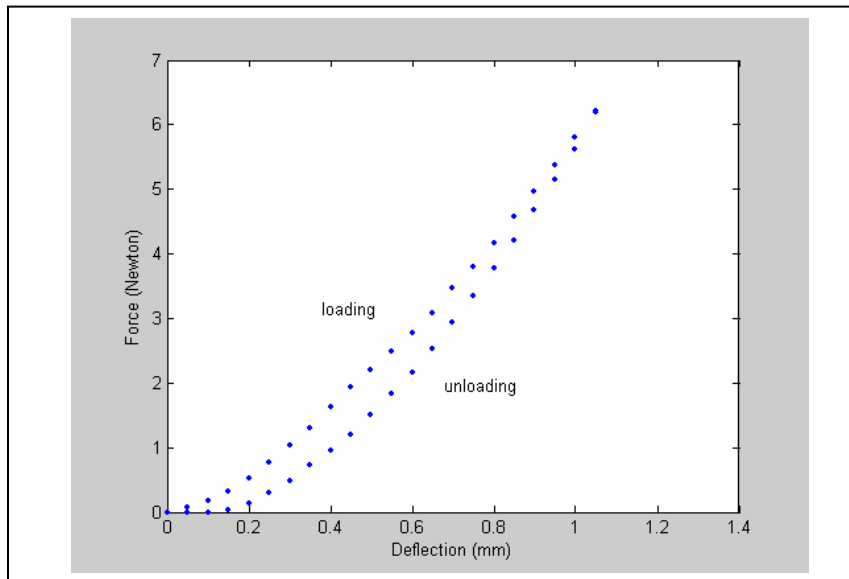
Figure 3.10: Force-displacement plot for sample C

3.4 Static Experiments of One-Layer Panels

Tests were also performed on a set of one-layer panels. Several one-layer panels made of circular cone stiffeners (referred to as Samples C1-C4) and hexagonal cone stiffeners (referred to as Sample H) were tested. Stiffener geometries are seen in Figure 3.11.
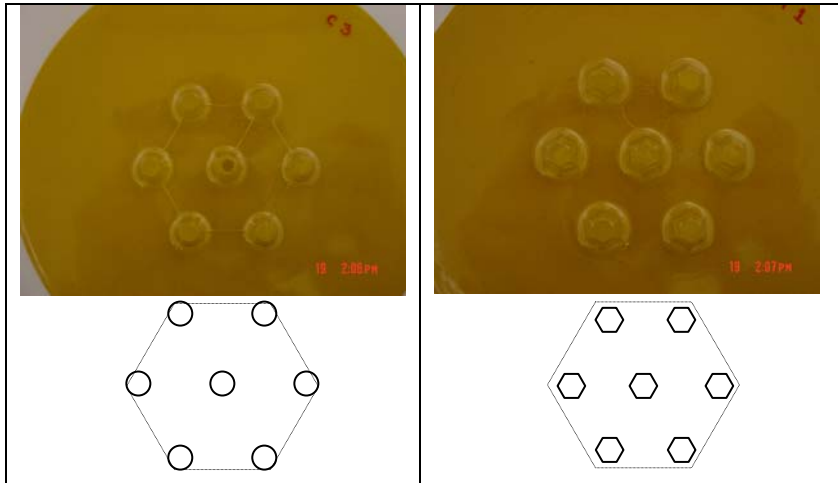
Figure 3.11: Circular cone and hexagonal cone samples

Four configurations for sample C were tested. The details of the configurations and dimensional details are presented in Table 3.2. A pictorial comparison of different configurations of sample C is presented in Figure 3.12.

Table 3.2: Dimensional variations of the one-layer samples

Sample	Radius 'r'	Height 'h'
C 1	3.175 mm	4.96 mm
C 2	3.175 mm	4.96 mm
C 3	3.175 mm	11.9 mm
C 4	12.7 mm	9.9 mm
H 1	12.7 mm	11.9 mm
H 2	12.7 mm	11.9 mm

Sample C1
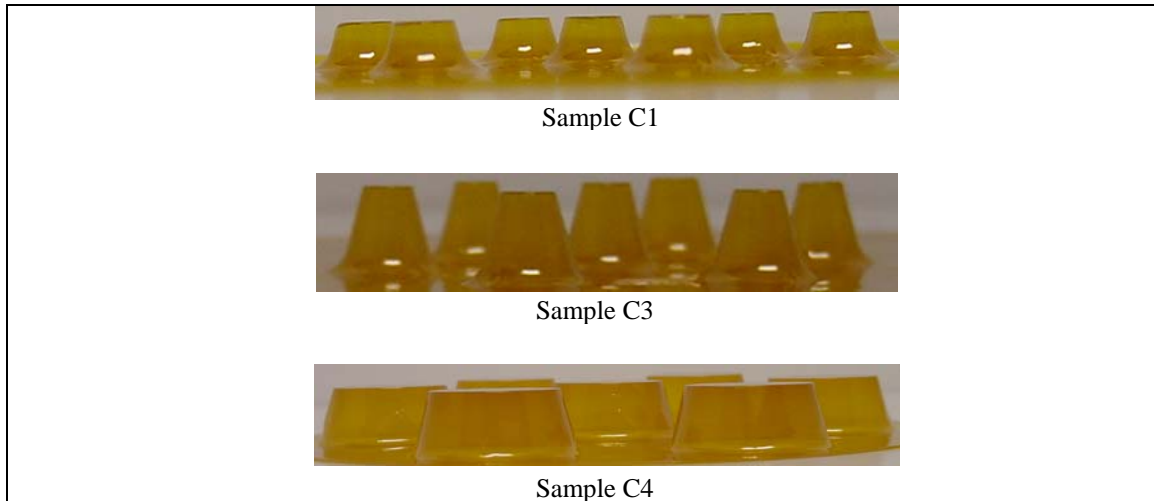
Sample C3

Sample C4

Figure 3.12: Height and radius comparison of conical stiffener

As the one-layer conical and hexagonal samples were much less stiff than the samples described in Table 3.1, a different test procedure was used. Figure 3.13 shows the experimental test setup that was used to perform this test. Samples were mounted on a flat surface and loads were applied on a flat plate placed on top of the stiffener cones on the samples. The displacement of the cones due to the applied load was measured from the bottom using a laser sensor. The test data is presented in Appendix 2.
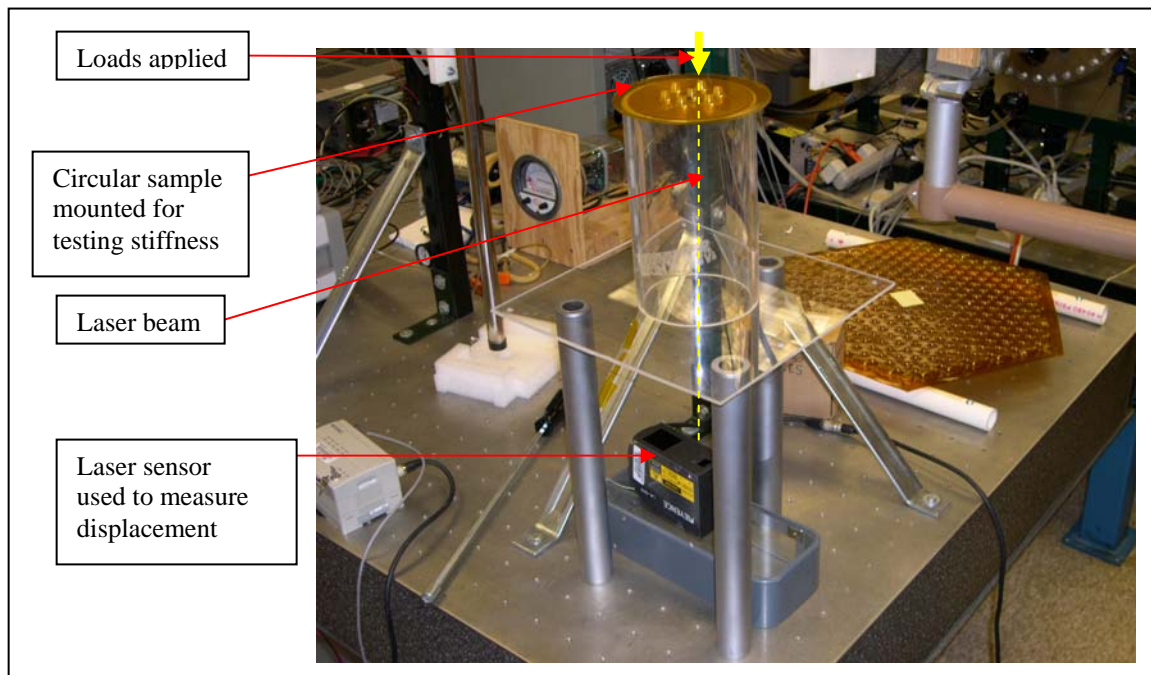
Figure 3.13: Experimental setup for testing round samples

Figure 3.14 shows the force-displacement plots for samples C1, C2, C3, C4 and sample H (refer to table 3.2). The displacements are plotted only for the loading cycle. It was not possible to record the displacements for the unloading cycle because only very minor variations were noticed during unloading and the experimental setup was not accurate to capture these small variations. The loads were applied using 20g, 50g, 100g, and 200g masses respectively. As it was difficult to get accurate results for each load, the tests were repeated three times. As only three displacements were recorded for each data set, the plots in Figure 3.13 are the curve fit for the data points recorded. Samples C1 and C2 are plotted together and samples H1 and H2 are plotted together. Based on the results seen, the test procedure adopted to test these samples was questioned and also, varying bilinear trends were seen. More study with a different experimental procedure is recommended for these samples.
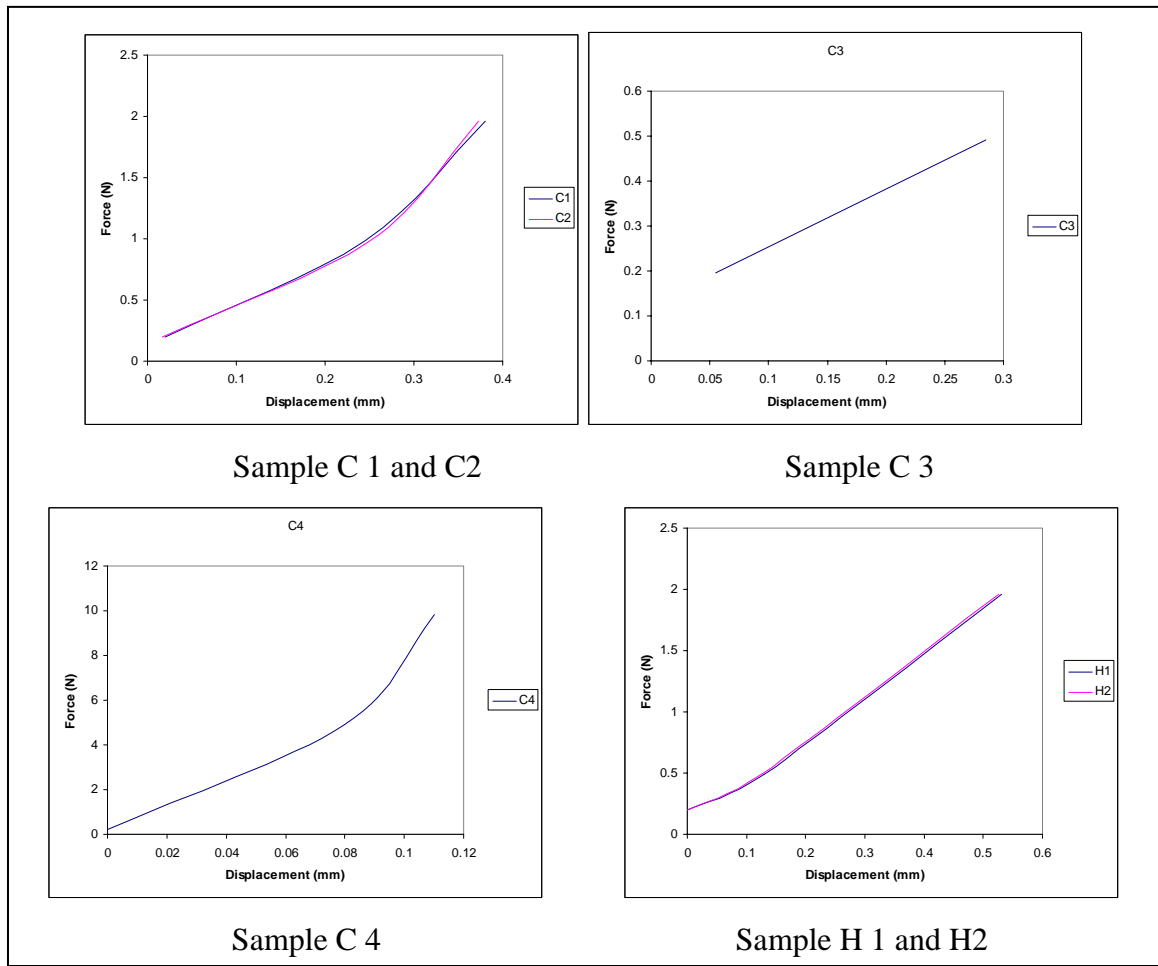
Figure 3.14: Force-displacement plots for samples C1, C2, C3, C4, H1 and H2

3.5 Static Experiments of Two-Layer Full Panel

A different test procedure was adopted for performing the static test on the full panel. The panel was mounted in such a way to approximate a standard beam bending test with simply supported boundary condition on two sides using circular supports. Double-sided tapes lightly secured the panel to the supports to ensure that it did not lose contact with the surface while applying loads. This is presented in Figure 3.15.
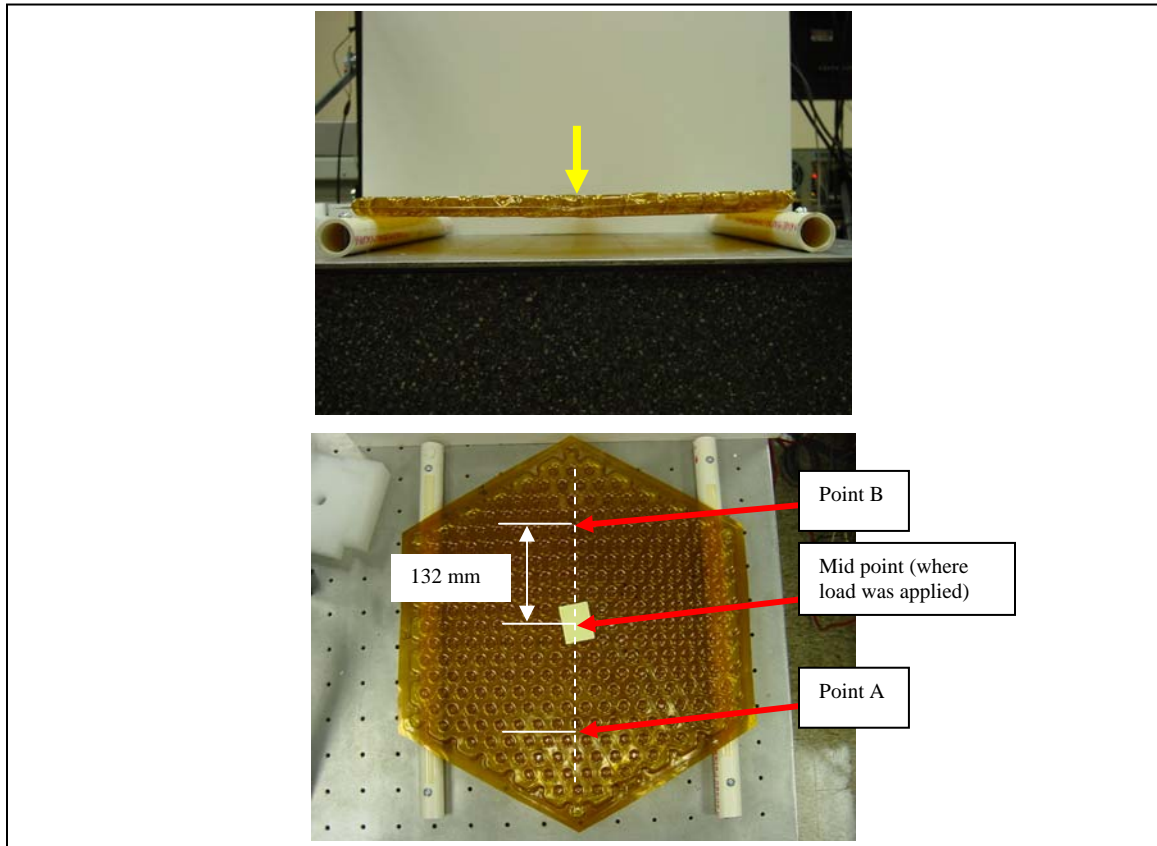
Figure 3.15: Panel setup for static test

The center of the panel was located and static loads were applied at this point. Laboratory hanging masses were used to apply the load from 0.0981 N (10 g mass) through 0.981 N (100g mass) in increments of 0.0981 N. Two points A and B were located 132 mm from the center as shown in figure 3.14. The vertical displacement of A was measured for each load step with a laser sensor. The laser sensor was mounted above the panel and adjusted so that the beam was focused on point A. The same was repeated for point B. A computer based data acquisition system was used to record the output of the laser sensor. Figure 3.15 presents the entire setup that was used to perform this test.
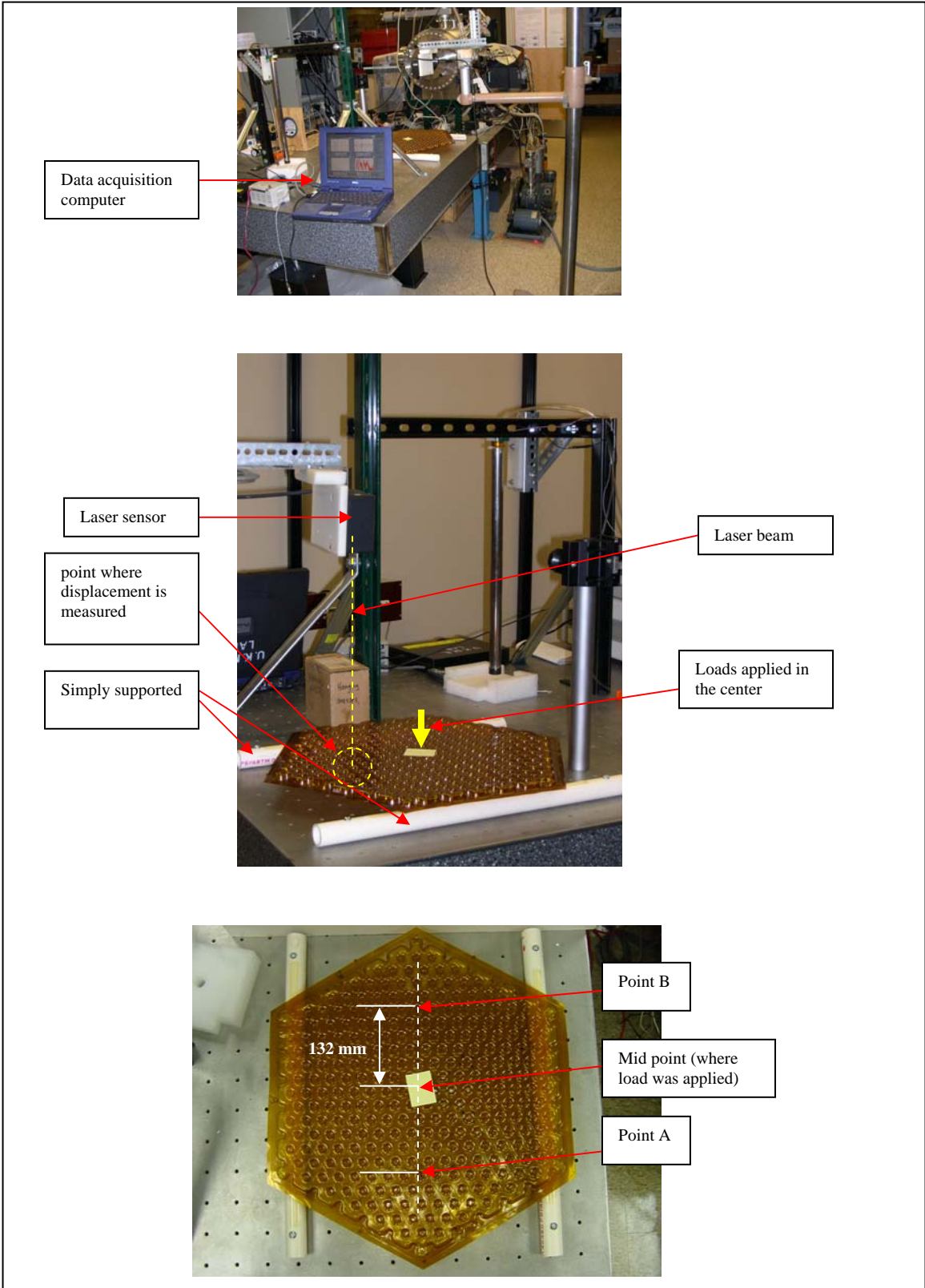
Figure 3.16: Experimental setup for full panel static test

As can be seen in Figure 3.16, the panel was supported on two sides on the stiffener units and not on the flanges. This was done because the bending property of the panel was the main focus of the experiment and not the flange bending properties.

The maximum loading range was limited to 0.981 N for this test. For higher loads (1.2 N and higher), a distinct click sound was heard from the panel stiffener units indicating local buckling of the stiffener units. The test was repeated three times for each point with no appreciable difference in results.

The force-displacement plots for the panel are presented in Figure 3.17 and all the test data is presented in Appendix 3. Plots of the data for both points are compared in Figure 3.17. It can be seen that at Point A, the panel behaved approximately linearly over the entire range of loading. However at Point B, the panel tends to soften approximately after a load of 0.6 N.
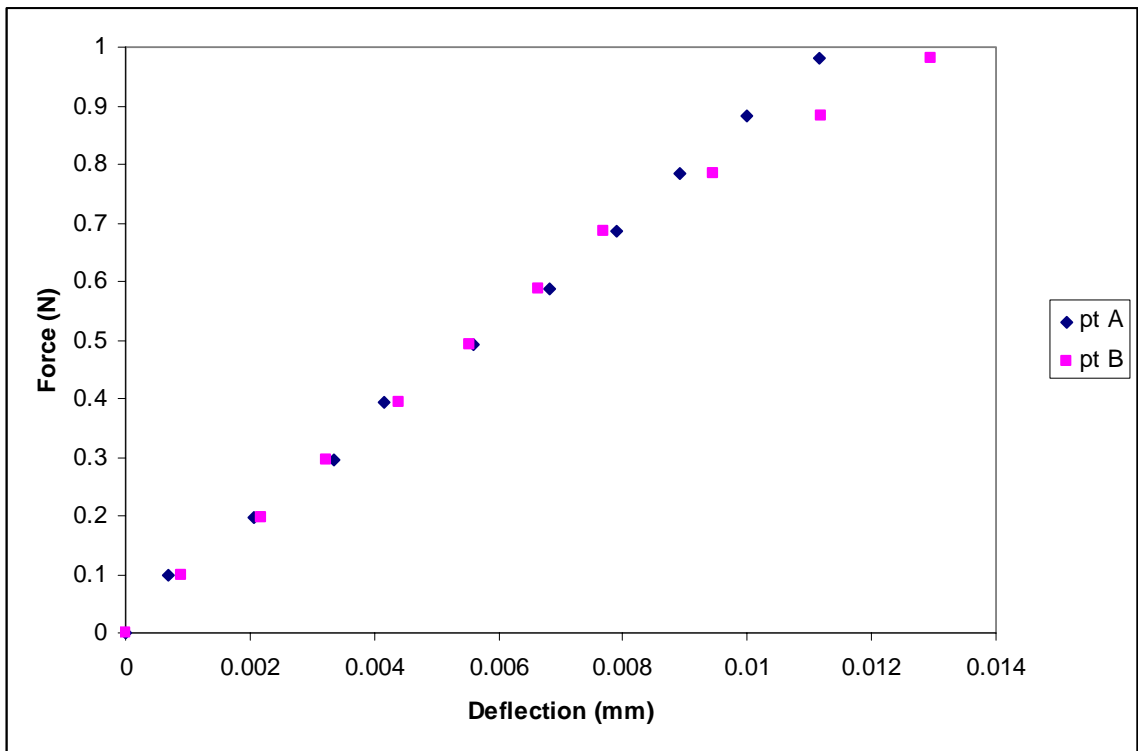
Figure 3.17: Force-displacement plots for points A and B for full panel

3.6 Results Summary

The force-displacement plots in Figures 3.6 and 3.7 indicate that the single layer conical stiffener units exhibit approximately linear stiffness. However, Figure 3.8 shows that the two-layer stiffener unit exhibits hardening characteristics that can be approximated as a bilinear static response. This, combined with the qualitative observation of deformation of the stiffener unit suggests that they could be modeled using spring elements, either a single spring with experimental force-displacement characteristics of the two-layer stiffener unit or two springs in series with experimental force-displacement characteristics of the individual single layer conical stiffener units. It is also seen from Figure 3.8 that the stiffness of the two layer stiffener unit in the steeper part of the curve is higher than the calculated stiffness using the top and bottom cone in series. A similar behavior is seen in Figure 3.10 where the stiffness of the four-unit panel is about 20% more than the calculated value.

Further, the plots in Figure 3.17 indicate that the panel behaves approximately linearly over the entire load range for both points tested. Apparently, the bilinear behavior of the individual stiffener units is diminished when a number of individual units act in parallel. Details of the finite element modeling process and the comparison of the model behavior with the tested sample behavior, along with further discussion of the nonlinear characteristics of the structure, are presented in Chapter 4.

CHAPTER FOUR

Finite Element Modeling

4.1 Introduction

This chapter presents a description of the process of developing finite element (FE) models of the panel units discussed in the previous chapter. It presents the approach used to arrive at a FE model for the complete panel. Sections of this chapter present the types of elements used for the model and their characteristics. The boundary conditions and the type of loading applied to the model are also discussed. Finally, the results of the static analysis performed on the FE model of the two-layer panel are presented.

4.2 Finite Element Modeling

As seen in the previous chapter, the stiffening units display nonlinear characteristics when subjected to loading. One approach to modeling these stiffeners would be to develop detailed models including material complexities and other intricate details. However, this could lead to a model with too many dofs to be useful for design. The second approach would be to model the stiffeners as nonlinear spring elements. This approach would be a more practical and simplistic approach.

The second approach was chosen to develop finite element models of the individual stiffener units. Based on this approach, the panels units are modeled as nonlinear springs with either two or three nodes. The outer-surface Kapton sheets connecting the stiffener units are modeled as shell elements with corner nodes. The thinner sheet of Kapton present in between the two cones in the tested sample (refer to Figure 3.3) is not represented in the corresponding FE model as its primary purpose is to provide a surface for bonding the two cones together. The full panel does not include this thin intermediate sheet. A detailed description of the panel modeling based on this approach is presented in the following sections.

4.3 Modeling Individual Stiffener Units

Based on the static displacement experiments that were conducted on different sets of individual stiffener elements described in Chapter 3, two FE models were developed to represent the panel stiffener units. Two approaches were considered for modeling the stiffener elements: 1) Model 1 was to model the top and bottom cones using different nonlinear spring elements and then use a serial combination of these springs to represent the two-layer, one-unit stiffener and 2) Model 2 was to model the two-layer, one-unit stiffener as a single nonlinear spring.

4.3.1 Description of Two-Spring and One-Spring Models of Stiffener Unit

Figure 4.1 presents a representation of the two-spring and the one-spring models. A pictorial representation of stiffener unit is also presented. The two-spring model has three nodes and the one-spring model has two nodes. The FE model of the two-layer, one-unit stiffener using Model 1 is presented in Figure 4.2 and the FE model using Model 2 is presented in Figure 4.3.
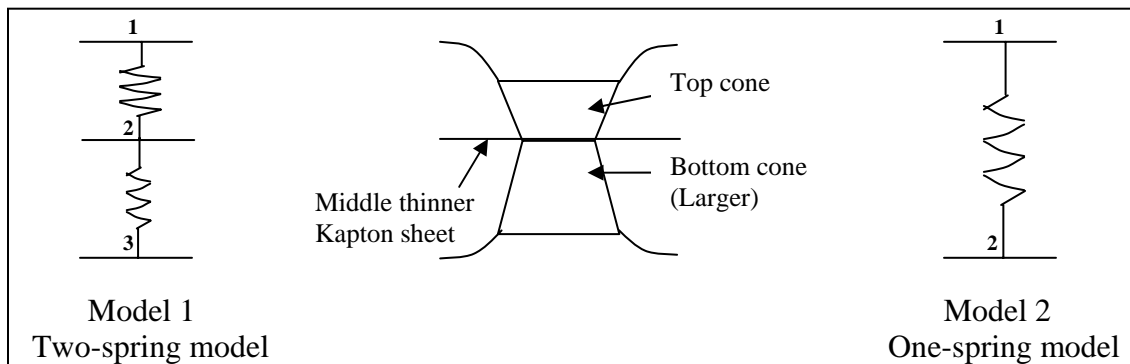
Figure 4.1: Two-spring model (left) and one-spring model (right) of two-layer, one-unit stiffener
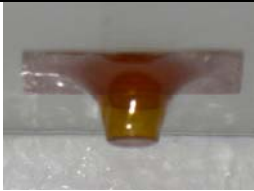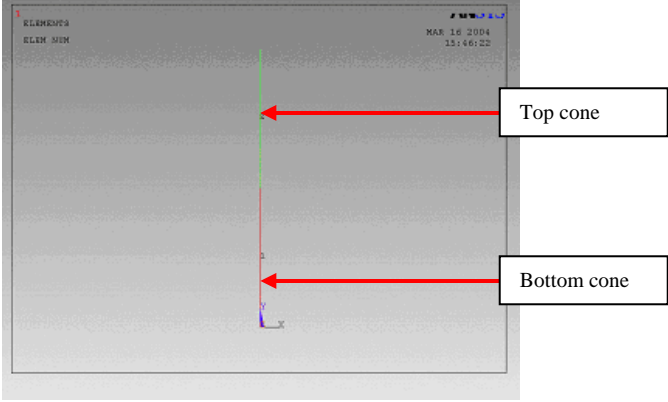
	Bottom cone	Top cone
Stiffness	See Fig 3.7 for force-disp. relationship	See Fig 3.6 for force-disp. relationship
Two-spring FE model		

Figure 4.2: FE model of two-layer, one-unit stiffener using Model 1
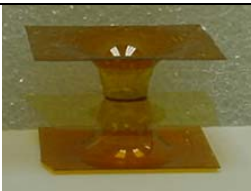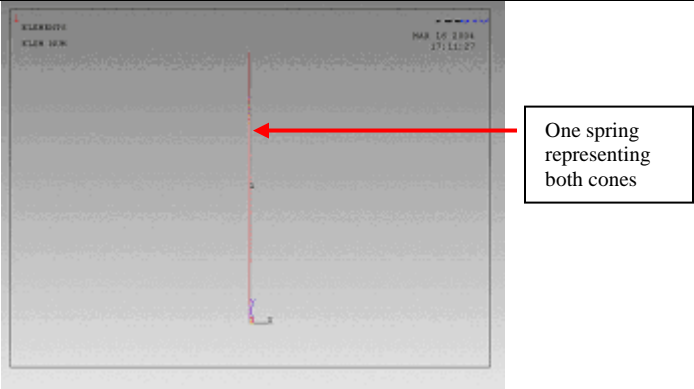
	One unit sample (bottom and top cones together)
Stiffness	see Fig 3.8 for force-disp. relationship
One-spring FE model	

Figure 4.3: FE model of two-layer, one-unit stiffener using Model 2

The ANSYS version 8.0 nonlinear spring element (COMBIN39) was used to model the individual panel units. COMBIN39 is a unidirectional element with nonlinear generalized force-deflection capability that can be used in any analysis. The element has longitudinal or torsional capability in 1-D, 2-D, or 3-D applications. The element has one dof at each node in the axial direction. Experimental results obtained from static deflection tests performed on different sets of individual stiffener units were used to define the element properties in the axial direction. Refer to Section 3.4.1 for details of how the spring properties were measured.

4.4 Modeling a Multiple-Stiffener Sample

For each model of the individual stiffener units (Model 1 and Model 2), a four-unit panel model was developed. This was done by using parallel combinations of Model 1 and Model 2 respectively. Two surfaces were generated to connect the top spring nodes and the bottom spring nodes respectively. The top and the bottom surface surfaces were meshed using the auto-mesh feature in ANSYS to generate shell elements representing the Kapton sheets connecting the cones. For static analysis of the four-unit-two-layer model, the shell elements did not contribute to the stiffness behavior as loads were applied to the top spring nodes only. Results of static analysis of the four-unit model were compared to the results of static testing on the four-unit sample. This intermediate step was performed to provide phased validation of the FE model with respect to the tested sample. Figure 4.4 presents a pictorial representation of the four-unit panel and the corresponding FE models.

Multi-unit sample C	FE model of panel	
	Model 1: two-spring model	Model 2: one-spring model
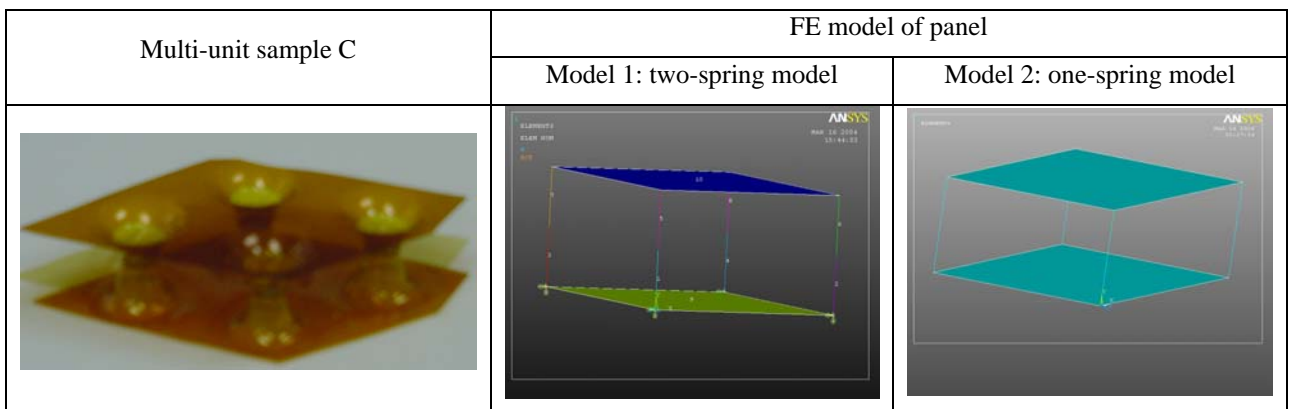
Figure 4.4: Physical model and FE model of four-unit panel

In addition to the spring elements in Section 4.3.1, the model includes shell elements (SHELL 63) for the top and bottom layers of the multi-unit sample. SHELL 63 has both bending and membrane capabilities. The element has six degrees of freedom at each node. A thickness of 0.127 mm (5 mil) was used for the shell elements composing the top and bottom Kapton layers of the sample. This was obtained by measuring the thickness of the Kapton sheet in the tested sample. Table 4.1 lists the physical properties of Kapton that were used for the model.

Table 4.1: Physical properties of Kapton

Property	Value
Tensile Modulus	2.5 G Pa
Poisson's ratio	0.34
Density	1.42 E3 Kg/m³

The bottom nodes of the four-unit model were constrained in all directions while the top nodes were free to translate in only the vertical direction. Loads were applied in the vertically downward direction as presented in Figure 4.5 and the corresponding displacements were recorded. A two-spring representation of the panel stiffeners is shown in this figure.
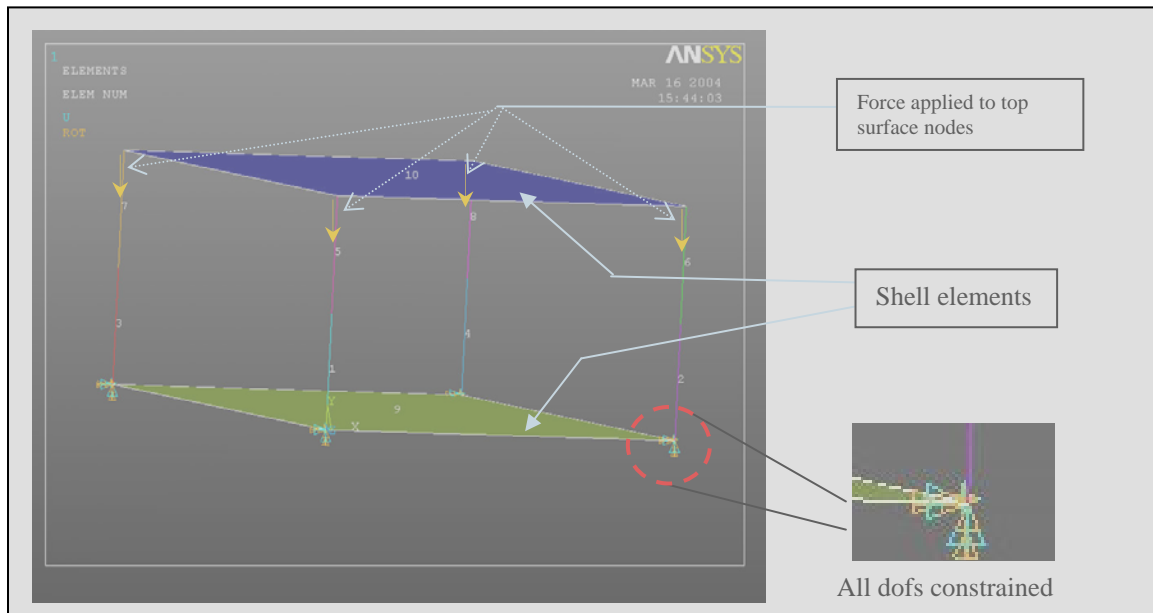
Figure 4.5: FE model of four unit panel showing loads and boundary conditions

Figure 4.6 shows the results of the static analysis with the four-unit models using a two-spring stiffener (Model 1) and a one-spring stiffener (Model 2) plotted with the static test results. The displacement in mm is plotted in the horizontal axis and the force in Newtons is plotted in the vertical axis. From Figure 4.6 it can be seen that the results of FE Model 2 show more pronounced nonlinear behavior in the region from 0 to 0.2 mm displacement than FE Model 1. FE Model 2 has a distinctly changing slope from a stiffness less than that of FE Model 1 to a stiffness approximately 33% greater than that of FE Model 1. The experimental results also exhibit a distinct change in slope, but in the region 0 to 0.4 mm displacement. The results of FE Model 1 exhibit a less-changing slope, with the final stiffness more parallel to the experimental result.
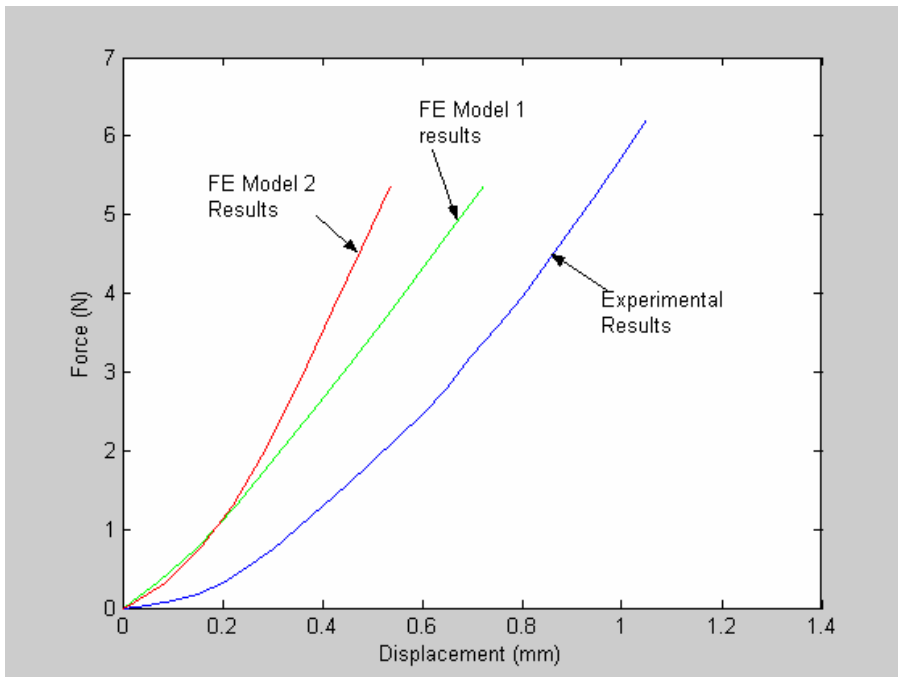
Figure 4.6: FE model results compared to static test results for four-unit panel.

The stiffness of the lower portion of the experimental results plot in Figure 4.6 is approximately 2 N/mm and the steeper portion of this plot is approximately 10 N/mm compared with slopes of 1.5 N/mm and 3 N/mm of the one-unit stiffener in Figure 3.8 respectively. In parallel, the stiffness of the four-unit panel should be about 4 times the stiffness of one-unit stiffener. From the results of the static experiment performed on the four-unit test sample, it is noted that the structure stiffens beyond a certain load. A similar

behavior is also seen in the FE results of Model 2 (one-spring model). To include this nonlinear behavior, Model 2 was selected for use in the full-panel FE model. Additional efforts are needed to better correlate the four-unit models to the experimental results.

4.5 Modeling the Complete Panel

Based on the observation from the four-unit sample model, the complete panel was modeled using multiple one-spring stiffener units spaced in a hexagonal honeycomb-pattern. Figure 4.7 shows the FE model of the full panel. The nonlinear spring elements and the shell elements used to connect them are highlighted. The FE model is comprised of 241 spring elements and 10,801 shell elements. The batch file (ANSYS data input file) used to create the model of the full panel is presented in Appendix 5. The flanges of the panel were not included in the model at first, as the bending characteristics of the flanges was thought not to be of interest. The nodes on two parallel edges 1 and 2 of the lower surface were constrained in translation. Loads were applied to the center node of the top surface and the vertical deflection of the nodes corresponding to points A and B in the actual panel (see Figure 3.15) were recorded.
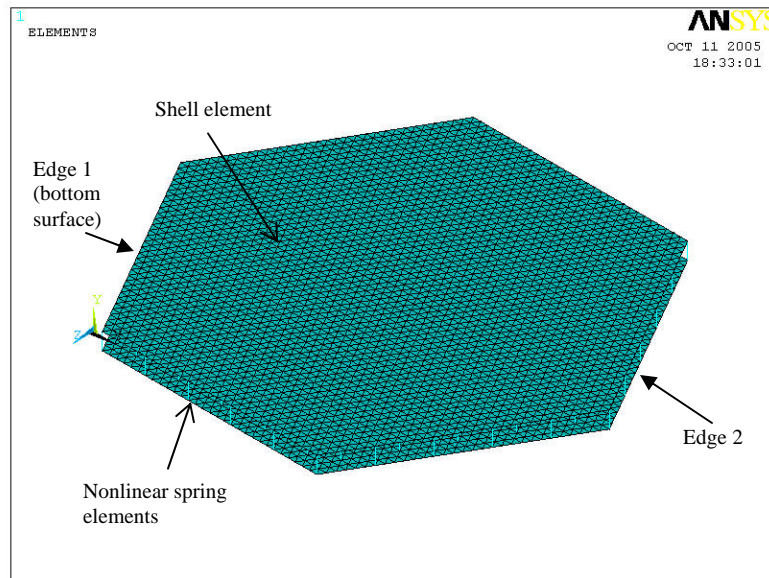
Figure 4.7: FE model of complete panel using one-spring model
(Model 2) for each stiffener unit

38

The results of the static analysis on the full panel are presented in Figure 4.8 in comparison with the results of the static experiment. The data for the static analysis on the full panel is presented in Appendix 6. The deflection in mm is plotted on the horizontal axis and the force in Newtons is plotted on the vertical axis. The plot indicates that the FE model results and the test results follow a linear trend. The FE model was considered a sufficiently accurate representation of the full panel in static analysis to continue to the dynamic analysis effort.

The nonlinearly increasing stiffness observed from the data of the four unit panel model seems to have diminished significantly in the full panel model and in the full panel experiment. However, the test results still show a slight softening trend of the panel as the load increases. From these results it is theorized that in thermoform-stiffened panel structures the effect of nonlinearities localized in individual stiffeners is diminished when many such stiffeners combine to form the complete panel.
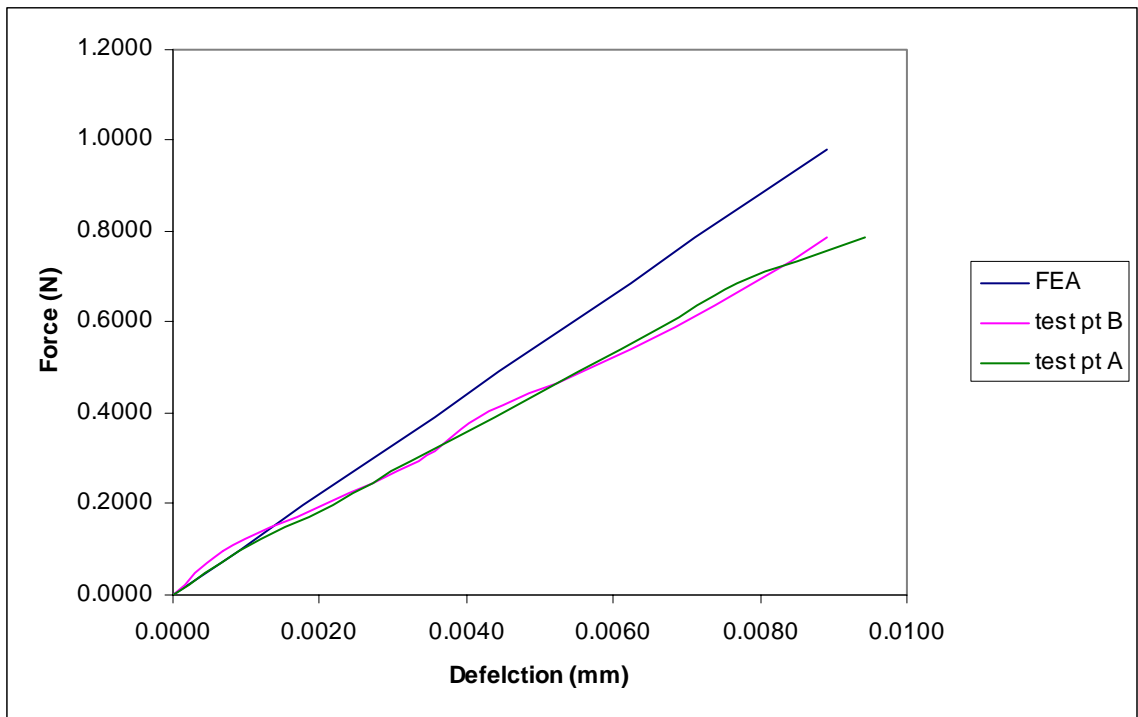
Figure 4.8: Comparison of FE Analysis and experimental results for static analysis on full panel

Dynamic testing was performed to further compare the behavior of the model when subjected to dynamic loads. The following chapter describes the details of dynamic testing and dynamic analysis performed on the complete model.

CHAPTER FIVE

Dynamic Experimentation and Modeling

5.1 Introduction

This chapter presents the details of modal testing that was performed on the panel. The experimental setup and test procedure are explained in detail. The second part of this chapter includes details of the finite element modal analysis that was performed with several full panel models. Plots for different mode shapes are presented. The results of the physical testing and the FE model analysis are then compared.

5.2 Modal Tests on Full Panel

Modal testing was performed on the panel using standard modal testing practices as possible, with modifications as needed. Figure 5.1 shows the test setup that was used to perform the modal testing. The panel was suspended by two mono-filament lines, each 400 mm long. This was to approximate free-free boundary conditions and to minimize the effect of rigid body modes on the elastic mode response between 0-100 Hz.
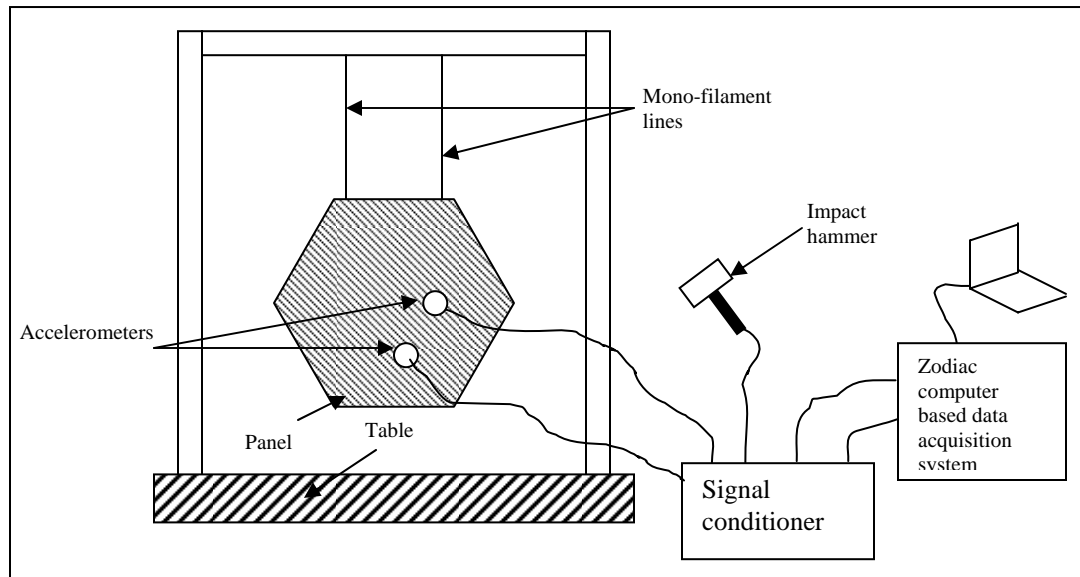
Figure 5.1: Test setup for panel modal testing

A conventional single point impact hammer (PCB 086B01) was modified by attaching a rectangular aluminum plate measuring 38.1 mm in width and 101.6 mm in length to its tip in order to mitigate local deformation on the panel at the point of impact. Griffith recognized the effect of local deformation when testing an inflatable torus with impact hammer excitation and used a similar modification for his hammer input [14]. Figure 5.2 shows the impact hammer and plate used to excite the panel for modal testing.

Figure 5.2: Impact hammer and aluminum plate

The vibration response of the panel was measured at 24 different points using a 2-g small-mass accelerometer (PCB Model A353A16) with a nominal voltage sensitivity of 10mV/g and a frequency range between 1 – 10,000 Hz. A second accelerometer was used as a reference. The reference accelerometer was located in the center of the panel behind the point where excitation impact was applied. The location of the response accelerometer was changed to different predefined points during the course of testing to be able to compute the frequency response for different points on the panel. Figure 5.3 shows the location of the predefined points numbered in the clockwise direction starting from the inner blue points to the outer red points.
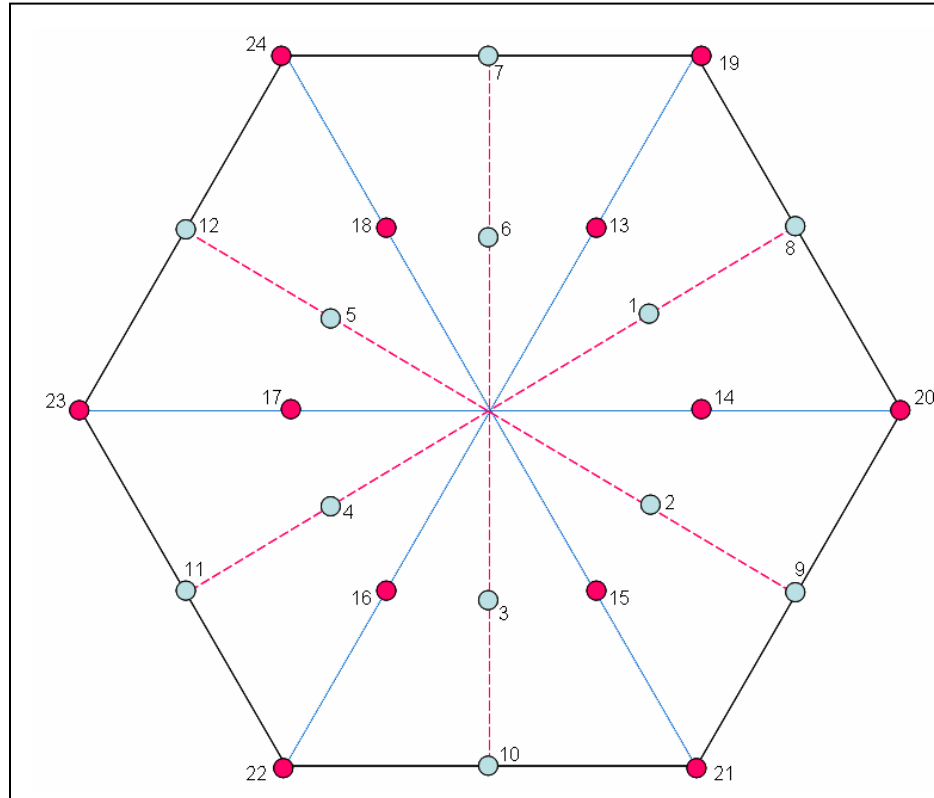
Figure 5.3: Pre-defined accelerometer locations

The input force time history data from the impact hammer and the output response time history from the accelerometer were recorded by a multi-channel mobile dynamic signal analyzer. A sampling rate of 200 samples per second was used. Preliminary testing showed that five averages were sufficient for this test. The frequency response functions were determined at 24 points using by the single-input single-output (SISO) method. The panel was excited in the center for each test and the response was measured at points 1 through 24 in turn. For each location of the response accelerometer, the panel was excited five times and the average of the five readings was recorded as the final FRF. Averaging reduces the noise producing a more accurate FRF. FRF plots for response measured at 13 points are presented in Appendix 7. Figure 5.4 presents the FRF plots for location points 1, 3, 12 and 14.
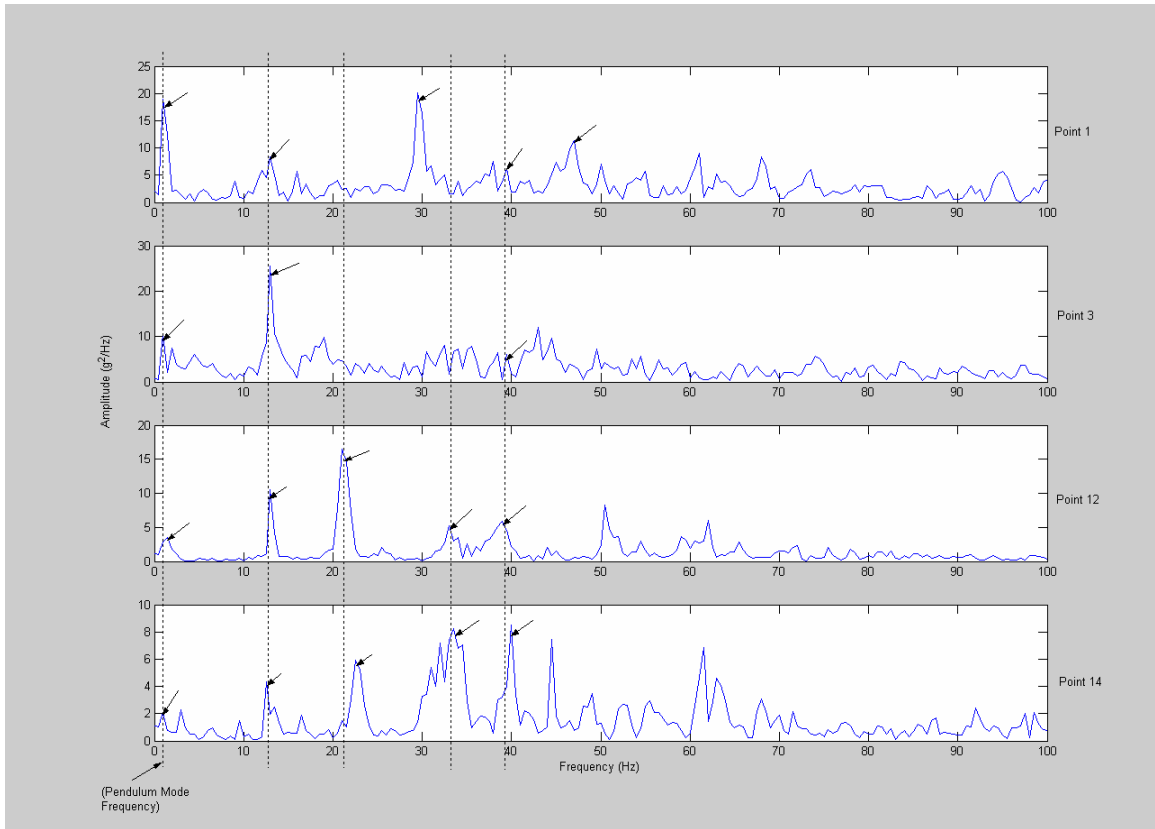
Figure 5.4: Typical better FRF for locations 1, 3, 12 and 14

Frequency in Hertz is plotted on the horizontal axis and amplitude in G^2/Hz is plotted on the vertical axis. Significant peaks are highlighted in the figure with dotted lines to show the comparison. The first peak in each plot is expected to be the pendulum mode of the panel swinging on the monofilament lines. This frequency was estimated using the panel dimension of 0.250 m from the top edge to the center and compared to the measured values in the FRFs. Table 5.1 presents the calculated and measured values of natural frequency for the pendulum mode.

Table 5.1: Comparison of natural frequency for pendulum mode

Calculated natural frequency in pendulum mode	Measured natural frequency in pendulum mode			
	Point 1	Point 3	Point 7	Point 12
0.63 Hz	1.4 Hz	1.5 Hz	1.4 Hz	1.4 Hz

After the pendulum mode, the next peaks seen in the FRFs are approximately at 12-12.5 Hz, 21-23 Hz, 29-35 Hz and 39-40 Hz respectively. Figure 5.5 presents two examples of low-quality FRF plots that were also recorded during the test. In these plots and others like them the averaged FRF does not show clear peaks typical of modal response.
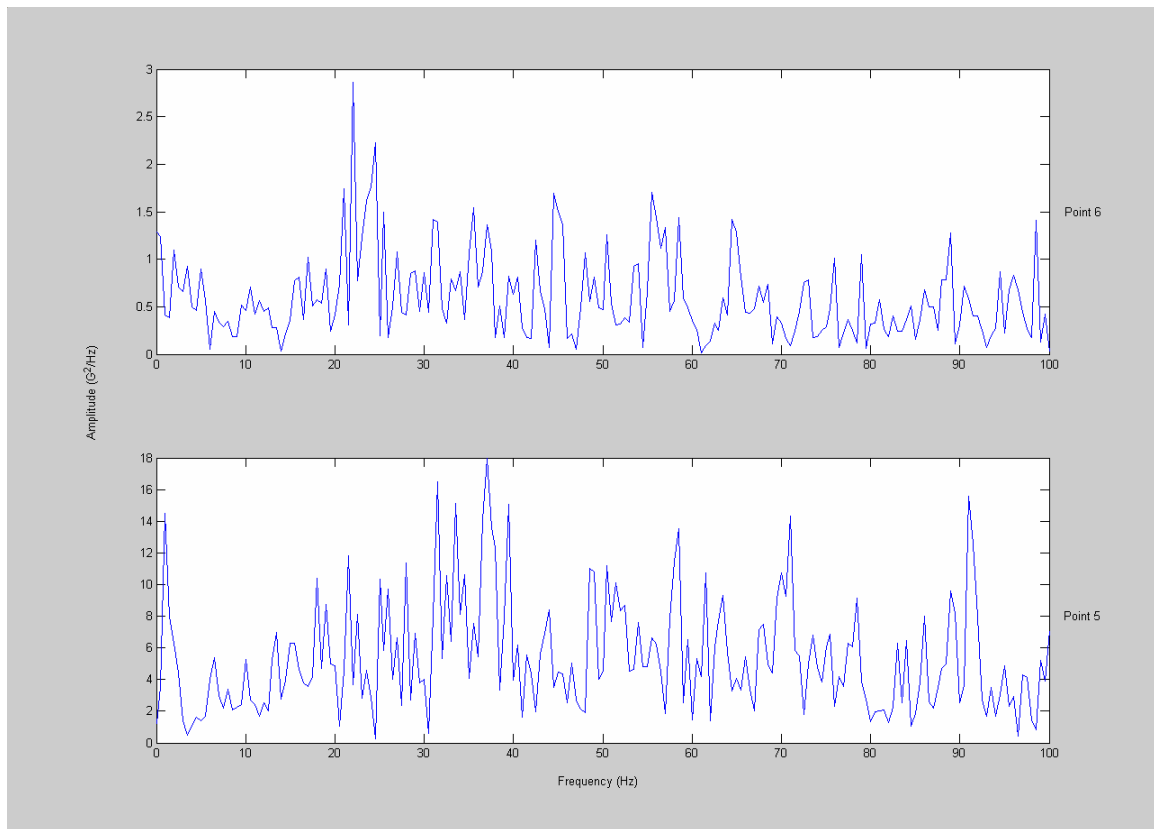
Figure 5.5: Bad FRF plots

Measured frequency response function data can be loaded into X-Modal software (modal analysis software) which can be used to identify modal quantities including natural frequencies, mode shapes and damping. The frequencies and mode shapes identified using X-Modal can be compared to those obtained from the modal analysis of the finite element model. However, the results of X-modal analysis are not available as this part of the original thesis plan was not completed. Another, less accurate method to compare the experimental response to that of the finite element model is to compare

natural frequencies. However, without mode shapes to compare, frequency matching is uncertain.

5.3 Modal Analysis of Finite Element Model of Full Panel

Modal analysis was performed using the finite element model of the full panel. For this analysis, the panel was not constrained at any boundary, but considered free-free. Natural frequencies and mode shapes were extracted with the Block Lanzcos method. From the modal testing results, several frequencies of interest were observed in the range of 0-50 Hz. Therefore, the first 20 modes in the frequency range of 0 – 100 Hz were computed. The frequency list included six rigid body modes, elastic bending modes and modes with relative movement between top and bottom surfaces. Modes 1 to 11 are rigid body modes combined with relative movement between top and bottom surfaces. Modes 13, 17 and 19 are distinct bending modes. Mode 13 and 14, 15 and 16 are orthogonal pairs. The frequencies of modes 13 to 20 are presented in Table 5.2. The frequencies and mode shapes of all 20 modes extracted are presented in Appendix 8. In modes 15, 16, 18 and 20, relative movement between the top and bottom surfaces occurs. This will not happen in reality because of the presence of the flanges connecting the top and bottom surfaces.

Table 5.2: Natural frequencies from modal analysis

Mode number	Frequency (Hz)	Description
13	33.5	Bending mode – saddle shaped
14	33.5	Orthogonal to 13
15	39.7	Relative movement between top and bottom surfaces
16	39.7	Orthogonal to 15
17	57.9	Bending mode
18	61.7	Relative movement between top and bottom surfaces
19	71.6	Bending mode
20	74.9	Relative movement between top and bottom surfaces

The mode shapes 13, 17 and 19 are presented in Figure 5.6. Mode 13 is a saddle-shaped bending mode at 33.5 Hz, Mode 17 is a breathing mode with a frequency of 57.9 Hz and

Mode 19 is another bending mode at 71.6 Hz. Modes 10, 11 and 18 are presented in Figure 5.7. In these modes, relative movement between the top and bottom surfaces occurs.
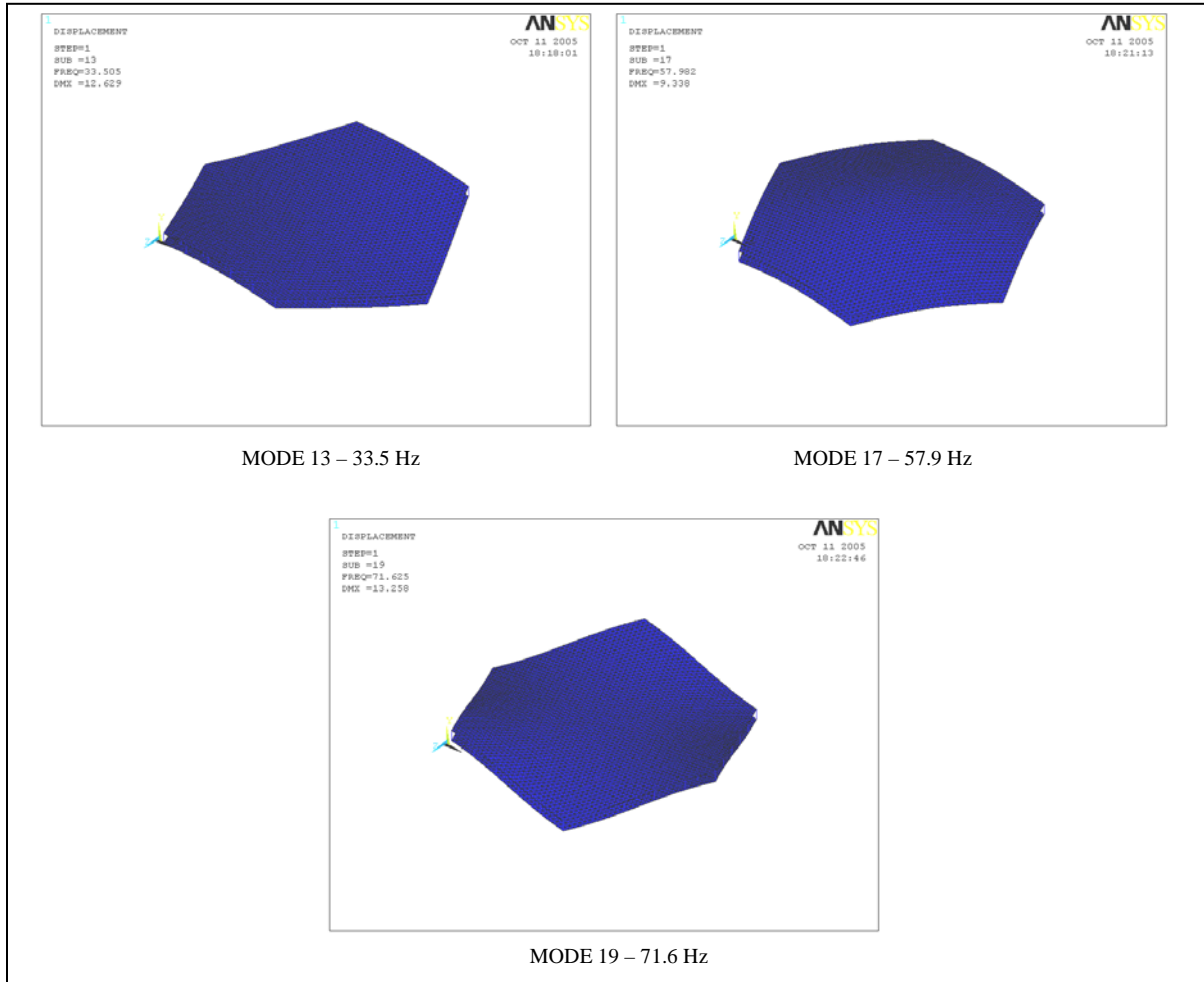

MODE 13 – 33.5 Hz

MODE 17 – 57.9 Hz

MODE 19 – 71.6 Hz

Figure 5.6: Mode shapes 13, 17 and 19

MODE 10 –20.1Hz

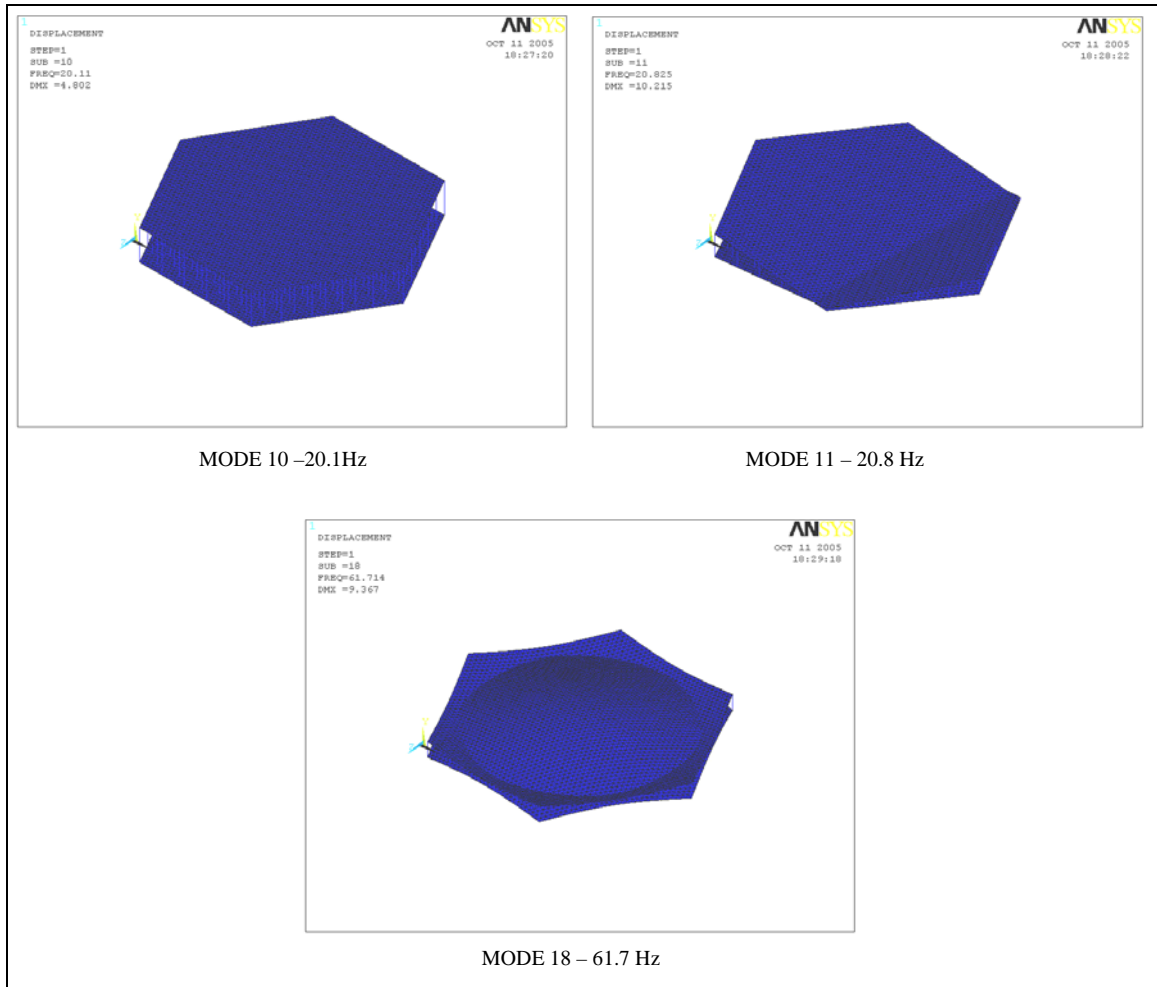MODE 11 – 20.8 Hz

MODE 18 – 61.7 Hz

Figure 5.7: Mode shapes 10, 11 and 18

Although static analysis of the full panel without the flanges resulted in accurate results, the modes showing out-of-phase motion of the top and bottom surfaces seen from modal analysis indicated that the presence of the flanges are needed to stabilize the top and the bottom surfaces. Thus, the FE model of the panel was modified to include the flanges connecting the top and bottom areas. Figure 5.8 shows the FE model with the flanges highlighted. The flanges were modeled with shell elements with thickness 0.254 mm, twice that of the top and bottom surfaces. The actual panel was comprised of two layers of Kapton glued together at the flanges. Modal analysis was performed on this modified model. However, except for the rigid body modes, all computed frequencies were above 100 Hz. The first elastic mode frequency occurred at 112 Hz. The modal test results of the panel seemed to indicate that some modal frequencies are between

0-100 Hz. The addition of the flanges to the FE model made it much stiffer than the actual panel. Since the frequencies of the panel model with the flanges were much higher than the actual frequencies, the flanges were not included.
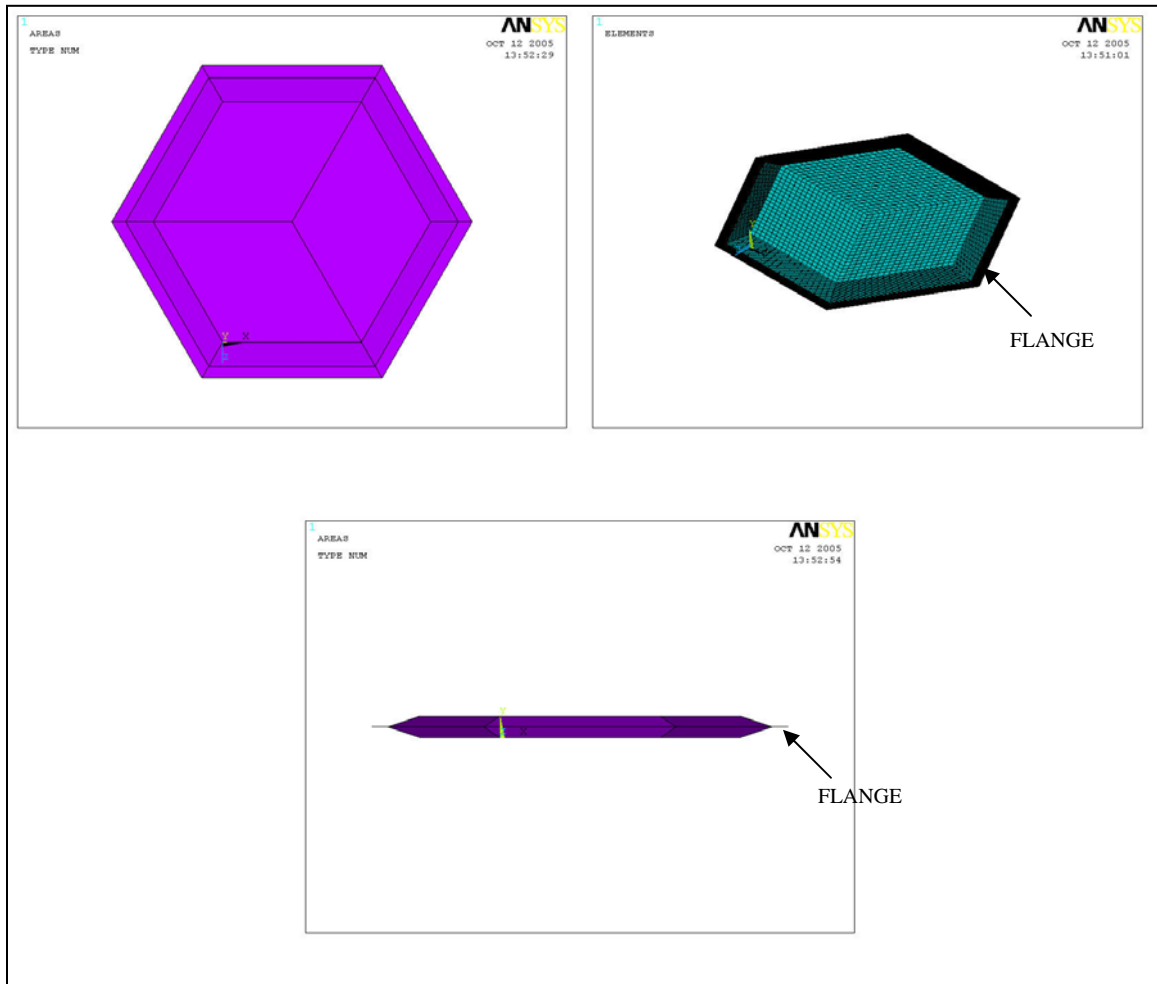
Figure 5.8: FE model of panel with flange

Another approach was tried to avoid the relative out-of-phase motion between the top and bottom surfaces. Springs with high stiffness (500 times the actual model spring, 2500 N/mm) were used to connect the top and bottom surfaces at the six corner nodes. This was done so that the top and bottom surfaces of the panel would move together. However, because the spring lacked stiffness in the lateral directions, this approach did not prevent all out-of-phase motions between the top and bottom areas.

5.4 Modal Analysis Summary

Table 5.3 presents a comparison of the frequencies from the FRFs and modal analysis. The pendulum mode (frequency 1.3 – 1.5 Hz) was seen in the testing due to the monofilament strings. These could also be added to the model for better comparison. Frequencies from the FRFs were obtained by the peak-picking method. As can be seen, the frequencies are comparable in terms of their numerical values, but without comparing the actual mode shapes, the comparison is not complete.

Table 5.3: Frequency comparison from FRF and modal analysis

Frequencies from FRF	Frequencies from modal analysis
1.3-1.5 Hz	-
21-23 Hz	20.110, 20.825 Hz
29-35 Hz	33.505 Hz
39-40 Hz	39.724 Hz

CHAPTER SIX

Thesis Summary

6.1 Summary and Conclusions

This chapter presents a comprehensive summary of this thesis. Recommendations for future work in the area of thermoformed stiffened panel structures are also included. The main objective of this thesis was to develop an understanding of the behavior of a thermoformed stiffened panel and to develop a finite element model of the panel based on static experimentation. The evaluation of the dynamic behavior of the panel was also of interest.

First, the smallest stiffener unit was tested. Static tests were performed and unit stiffness properties were established. Static tests were performed on each cone element of the unit stiffener to understand their individual properties and on the combined stiffener consisting of two cones. During the course of static testing, the mechanisms of deformation were also studied, providing a better understanding of the deformation phenomenon. Although each of the two cones behaves linearly in static tests of their stiffness under axial loading, the combination of these cones in a unit stiffener was seen to have a bi-linear stiffness. However, from the static test on a four-unit panel it was seen that bi-linear behavior diminishes when multiple unit stiffeners were combined. Both, hexagonal and circular configurations of the stiffener cone elements were tested.

Based on the results of static tests, two FE models were developed for the stiffener units using nonlinear springs; 1) one-spring model, 2) two-spring model. In the one-spring model, the stiffener unit was modeled as a single spring and in the two-spring model, two springs were used each representing the individual cones of the stiffener unit. A four-unit stiffener was modeled using the two modeling approaches. The analysis results of this model were compared with test results obtained by testing a four-unit panel

to find that the one-spring unit model produced a result with better qualitative correlation to test results. Neither model provided good qualitative correlation.

Based on this comparison, a full-panel model was developed using the one-spring model for each stiffener unit. Static tests were performed on the full panel and static analysis was done on the FE model of the full panel. The results of these tests and analysis were compared to find that the full panel model produced a result qualitatively and quantitatively comparable to the test results.

Modal testing was performed on the full panel and frequency response functions were determined. The frequencies of the analysis and the frequencies from frequency response function (obtained by peak picking) were compared. Modal testing revealed bending modes between frequencies 0-100 Hz.

Modal analysis was performed on the FE model and mode shapes and natural frequencies were extracted. Based on the analysis, the FE model was modified to include the side flanges connecting the two layers of the panel and this resulted in higher stiffness of the panel than indicated by the experimental results.

6.2 Conclusions

Although this thesis demonstrates that conventional testing principles could be applied to testing thermoformed stiffener panels. The phased-verification approach used in this thesis - where the full panel was broken down into smaller units and properties were established for these smaller units and then used to develop FE models for the full panel – can be extended to modeling and testing similar structures. The concept of using nonlinear springs to represent stiffener units for thermoformed stiffening units has been established during the course of this work. This reduces the need for in-depth modeling of similar structures thus making the idea of modeling extremely large structures feasible due to the limited number of nodes needed for such models compared to complicated models. This concept can be applied to similar stiffening structures.

6.3 Recommendations for Future Work

There are five main recommendations for future work related to thermoformed stiffener panels similar in construction to the panel discussed in this thesis.

First, a selection of stiffener units needs to be tested to document the range of behavior more completely. Further, the unit stiffeners should be tested with shear and torsional loading as well as axial loading as was done herein.

Second, a better way to represent the effect of the flanges connecting the top and bottom surfaces on the stiffness of the panel needs to be developed. The addition of the flange would stabilize the top and bottom surfaces and would eliminate the relative movement between them.

Third, the lateral stiffness of the panel needs to be measured by testing and this can be used to define lateral spring stiffness in the FE model. Lateral stiffness of the springs would add constraints on the movement of the spring nodes in the lateral direction.

Fourth, the damping characteristics of the panel need to be analyzed and measured. During this thesis, the damping properties of the panel were not measured. They were not accounted for in the finite element model. The effect of damping will affect the dynamic characteristics of the panel significantly.

Fifth, future testing of similar thermoform-stiffened ultra-lightweight panels should include static test on multiple-stiffener sample followed by static testing of individual stiffener unit cut from the multi-stiffener unit tested. Then the stiffener cones of the single-stiffener unit sample tested should be taken apart and tested separately. The results of these tests must then be compared. With this process, the elements comprising the tested assembly will be tested, rather than assuming similarity of unit stiffeners throughout.

APPENDIX 1

1. <u>Force-displacement results for sample A1 (Fig. 3.6 a)</u>

Displacement (mm)	Force (N)	
	Loading cycle	Unloading cycle
0.0000	0.0000	0.0000
0.0500	0.1711	0.0164
0.1000	0.3273	0.1023
0.1500	0.4978	0.2380
0.2000	0.6856	0.3849
0.2500	0.8682	0.5385
0.3000	1.0553	0.6804
0.3500	1.2558	0.8478
0.4000	1.4539	1.0176
0.4500	1.6563	1.2090
0.5000	1.8433	1.3711
0.5500	2.0470	1.5731
0.6000	2.2615	1.7791
0.6500	2.4834	2.0077
0.7000	2.6920	2.2201
0.7500	2.8990	2.4450
0.8000	3.0886	2.6742
0.8500	3.3003	2.9028
0.9000	3.4824	3.1463
0.9500	3.6715	3.3835
1.0000	3.8682	3.6399
1.0500	3.9091	3.9091

2. <u>Force-displacement results for sample A2 (Fig. 3.6 b)</u>

Displacement (mm)	Force (N)	
	Loading cycle	Unloading cycle
0.0000	0.0000	0.0000
0.0500	0.2673	0.0314
0.1000	0.5246	0.2192
0.1500	0.7774	0.4496
0.2000	1.0468	0.6768
0.2500	1.3191	0.8916
0.3000	1.5970	1.1220
0.3500	1.8816	1.3988
0.4000	2.1670	1.6666
0.4500	2.4396	1.9286
0.5000	2.6907	2.2261
0.5500	2.9244	2.4753
0.6000	3.1798	2.7626
0.6500	3.4357	3.0391
0.7000	3.6801	3.3252
0.7500	4.0009	3.6021
0.8000	4.2626	3.9200
0.8500	4.5182	4.2213
0.9000	4.8067	4.4846
0.9500	5.0640	4.8289
1.0000	5.2881	5.1308
1.0500	5.5272	5.5156

3. Force-displacement results for sample B (Fig. 3.7)

Displacement (mm)	Sample B 1 Force (N)		Sample B 2 Force (N)	
	Loading cycle	Unloading cycle	Loading cycle	Unloading cycle
0	0.0012	0.0000	0.0000	0.0000
0.05	0.0841	0.0000	0.0688	0.0000
0.1	0.1664	0.0368	0.1787	0.0032
0.15	0.2744	0.0867	0.2909	0.0674
0.2	0.3925	0.1589	0.4290	0.1490
0.25	0.5289	0.2592	0.5929	0.2511
0.3	0.6793	0.4034	0.7676	0.3857
0.35	0.8491	0.5532	0.9347	0.5397
0.4	1.0379	0.7151	1.1082	0.6449
0.45	1.2173	0.8579	1.2883	0.7794
0.5	1.3921	1.0287	1.4744	0.9261
0.55	1.5810	1.2091	1.5953	1.0422
0.6	1.7688	1.4116	1.7795	1.1339
0.65	1.9622	1.5661	1.9817	1.2708
0.7	2.1545	1.7657	2.1474	1.4022
0.75	2.3109	1.9639	2.2949	1.5217
0.8	2.4808	2.1650	2.4283	1.6618
0.85	2.6482	2.3915	2.5387	1.7653
0.9	2.8326	2.5794	2.6527	1.8937
0.95	3.0012	2.7907	2.6907	2.0169
1	3.1330	3.0199	2.7036	2.1572
1.05	3.2511	3.2428	2.7718	2.3123

4. Force-displacement results for sample C (Fig. 3.8)

Displacement (mm)	Force (N)	
	Loading cycle	Unloading cycle
0.0000	0.0000	0.0000
0.0500	0.0767	0.0000
0.1000	0.1745	0.0000
0.1500	0.3244	0.0362
0.2000	0.5213	0.1289
0.2500	0.7598	0.2896
0.3000	1.0353	0.4740
0.3500	1.3073	0.7204
0.4000	1.6243	0.9616
0.4500	1.9293	1.1982
0.5000	2.2047	1.4997
0.5500	2.4939	1.8217
0.6000	2.7780	2.1598
0.6500	3.0812	2.5226
0.7000	3.4729	2.9376
0.7500	3.7960	3.3410
0.8000	4.1718	3.7679
0.8500	4.5669	4.2128
0.9000	4.9553	4.6845
0.9500	5.3797	5.1470
1.0000	5.8022	5.6197
1.0500	6.2082	6.2003

1. Force-displacement results for sample C1 (Fig. 3.13)

Displacement (mm)	Force (N)
0.02	0.1962
0.245	0.981
0.38	1.962

2. Force-displacement results for sample C2

Displacement (mm)	Force (N)
0.14	0.1962
0.21	0.981
0.25	1.962

3. Force-displacement results for sample C3

Displacement (mm)	Force (N)
0.055	0.1962
0.285	0.4905

4. Force-displacement results for sample C4

Displacement (mm)	Force (N)
0	0.1962
0.08	4.905
0.11	9.81

5. Force-displacement results for sample H1

Displacement (mm)	Force (N)
0	0.1962
0.13	0.4905
0.53	1.962

6. Force-displacement results for sample H2

Displacement (mm)	Force (N)
0.125	0.1962
0.131	0.4905
0.525	1.962

APPENDIX 3

1. Force-displacement results for full panel at point A (Fig. 3.16)

Force (N)	Displacement (mm)		
	Trial 1	Trial 2	Trial 3
0	0.0000	0.0000	0.0000
0.0981	0.0015	0.0010	0.0010
0.1962	0.0027	0.0018	0.0022
0.2943	0.0038	0.0028	0.0030
0.3924	0.0052	0.0041	0.0044
0.4905	0.0068	0.0051	0.0056
0.5886	0.0082	0.0065	0.0071
0.6867	0.0093	0.0077	0.0083
0.7848	0.0108	0.0092	0.0099
0.8829	0.0119	0.0104	0.0109
0.981	0.0132	0.0118	0.0122

2. Force-displacement results for full panel at point B

Force (N)	Displacement (mm)		
	Trial 1	Trial 2	Trial 3
0	0.0000	0.0000	0.0000
0.0981	0.0009	0.0009	0.0011
0.1962	0.0022	0.0021	0.0010
0.2943	0.0032	0.0032	0.0019
0.3924	0.0044	0.0043	0.0030
0.4905	0.0055	0.0054	0.0041
0.5886	0.0067	0.0055	0.0055
0.6867	0.0077	0.0073	0.0065
0.7848	0.0094	0.0088	0.0075
0.8829	0.0101	0.0103	0.0087
0.981	0.0112	0.0114	0.0097

APPENDIX 4

1. Force-displacement analysis results for model 1 four-unit test panel (Fig. 4.6)

Force (N)	Displacement (mm)
0	0
0.0767	0.0166
0.3244	0.0704
0.7598	0.1488
1.3073	0.2264
1.9293	0.307
2.4939	0.3782
3.0812	0.4519
3.7960	0.5399
4.5669	0.6315
5.3797	0.7248

2. Force-displacement analysis results for model 2 four-unit test panel

Force (N)	Displacement (mm)
0	0
0.0767	0.0281
0.3244	0.0913
0.7598	0.1549
1.3073	0.2142
1.9293	0.2694
2.4939	0.3145
3.0812	0.3618
3.7960	0.423
4.5669	0.4823
5.3797	0.5594

APPENDIX 5

The ANSYS batch file to model the full panel is included in this section.

```
/filenam,full_panel_static_analysis
/prep7
et,1,39
et,2,63
r,1,0,0.0000,0.05,0.0376,0.1,0.1016
rmore,0.15,0.1805,0.2,0.2757,0.25,0.3940
rmore,0.3,0.5414,0.35,0.7011,0.4,0.8765
rmore,0.45,1.0376,0.5,1.2104,0.55,1.3950
rmore,0.6,1.5902,0.65,1.7641,0.7,1.9601
rmore,0.75,2.1374,0.8,2.3229,0.85,2.5199
rmore,0.9,2.7060,0.95,2.8959
keyopt,1,1,0
keyopt,1,2,0
keyopt,1,3,2
keyopt,1,6,0
r,2,0.127,,,
csys,0
mp,ex,2,2.5E9
nuxy,2,.34
dens,2,1.42E-6
n,1,0,0,0
k,1,0,0,0
n,2,0,17.145,0
k,2,0,17.145,0
e,1,2
ngen,7,2,1,2,1,43.9940,0,0,,
kgen,7,1,2,1,43.9940,0,0,2,,
ngen,15,14,1,14,1,0,0,-25.4
kgen,15,1,14,1,0,0,-25.4,14
egen,7,2,1,,,,,,,,43.9940,0,0
egen,15,14,1,7,,,,,,,0,0,-25.4
n,211,21.9964,0,12.7
k,211,21.9964,0,12.7
n,212,21.9964,17.145,12.7
k,212,21.9964,17.145,12.7
e,211,212
ngen,6,2,211,212,1,43.9940,0,0
kgen,6,211,212,1,43.9940,0,0,2
ngen,16,12,211,222,1,0,0,-25.4
```

kgen,16,211,222,1,0,0,-25.4,12
egen,6,2,106,,,,,,,,43.9940,0,0
egen,16,12,106,111,,,,,,,0,0,-25.4
n,403,43.9928,0,25.4
k,403,43.9928,0,25.4
n,404,43.9928,17.145,25.4
k,404,43.9928,17.145,25.4
e,403,404
ngen,5,2,403,404,1,43.9940,0,0
kgen,5,403,404,1,43.9940,0,0,2
egen,5,2,202,,,,,,,,43.9940,0,0
n,413,43.9928,0,-381
k,413,43.9928,0,-381
n,414,43.9928,17.145,-381
k,414,43.9928,17.145,-381
e,413,414
ngen,5,2,413,414,1,43.9940,0,0
kgen,5,413,414,1,43.9940,0,0,2
egen,5,2,207,,,,,,,,43.9940,0,0
n,423,-21.997,0,-38.0999
k,423,-21.997,0,-38.0999
n,424,-21.997,17.145,-38.0999
k,424,-21.997,17.145,-38.0999
e,423,424
ngen,12,2,423,424,1,0,0,-25.4
kgen,12,423,424,1,0,0,-25.4,2
egen,12,2,212,,,,,,,,0,0,-25.4
ngen,2,24,423,446,1,307.95,0,0
kgen,2,423,446,1,307.95,0,0,24
egen,2,24,212,223,,,,,,,307.95,0,0
n,471,-43.9940,0,-76.2
k,471,-43.9940,0,-76.2
n,472,-43.9940,17.145,-76.2
k,472,-43.9940,17.145,-76.2
e,471,472
ngen,9,2,471,472,1,0,0,-25.4
kgen,9,471,472,1,0,0,-25.4,2
egen,9,2,236,,,,,,,,0,0,-25.4
ngen,2,18,471,488,1,351.952,0,0
kgen,2,471,488,1,351.952,0,0,18
egen,2,18,236,244,,,,,,,351.952,0,0
n,507,-65.991,0,-114.3
k,507,-65.991,0,-114.3
n,508,-65.991,17.145,-114.3
k,508,-65.991,17.145,-114.3
e,507,508

```
ngen,6,2,507,508,1,0,0,-25.4
kgen,6,507,508,1,0,0,-25.4,2
egen,6,2,254,,,,,,,,0,0,-25.4
ngen,2,12,507,518,1,395.946,0,0
kgen,2,507,518,1,395.946,0,0,12
egen,2,12,254,259,,,,,,,395.946,0,0
n,531,-87.988,0,-152.4
k,531,-87.988,0,-152.4
n,532,-87.988,17.145,-152.4
k,532,-87.988,17.145,-152.4
e,531,532
ngen,3,2,531,532,1,0,0,-25.4
kgen,3,531,532,1,0,0,-25.4,2
egen,3,2,266,,,,,,,,0,0,-25.4
ngen,2,6,531,536,1,439.94,0,0
kgen,2,531,536,1,439.94,0,0,6
egen,2,6,266,268,,,,,,,439.94,0,0
n,543,-117.988,0,-177.8
k,543,-117.988,0,-177.8
n,544,-117.988,17.145,-177.8
k,544,-117.988,17.145,-177.8
n,545,381.952,0,-177.8
k,545,381.952,0,-177.8
n,546,381.952,17.145,-177.8
k,546,381.952,17.145,-177.8
n,547,256.9964,0,-394.28
k,547,256.9964,0,-394.28
n,548,256.9964,17.145,-394.28
k,548,256.9964,17.145,-394.28
n,549,6.9964,0,37.98
k,549,6.9964,0,37.98
n,550,6.9964,17.145,37.98
k,550,6.9964,17.145,37.98
n,551,256.9964,0,37.98
k,551,256.9964,0,37.98
n,552,256.9964,17.145,37.98
k,552,256.9964,17.145,37.98
n,553,6.9964,0,-394.28
k,553,6.9964,0,-394.28
n,554,6.9964,17.145,-394.28
k,554,6.9964,17.145,-394.28
edele,202,212,1
edele,7,,
edele,244,245,1
edele,268,269,1
edele,259,260,1
```

```
edele,223,224,1
edele,235,236,1
edele,253,254,1
edele,265,266,1
edele,1,,
edele,99,,
edele,271,,
edele,105,,
a,221,539,401,391,533,211
a,222,540,402,392,534,212
lsel,all
lesize,all,,,30,,,,,
type,2
real,2
mat,2
mshape,1,2-D
mshkey,0
amesh,all
nummrg,node,8e-3
allsel
```

APPENDIX 6

1. Force-displacement analysis results for full panel (Fig. 4.8).

Force (N)	Displacement (mm)
0.0000	0.0000
0.0981	0.0009
0.1962	0.0018
0.2943	0.0027
0.3924	0.0036
0.4905	0.0045
0.5886	0.0053
0.6867	0.0062
0.7848	0.0071
0.8829	0.0080
0.9810	0.0089

1. FRF measured at point 1:
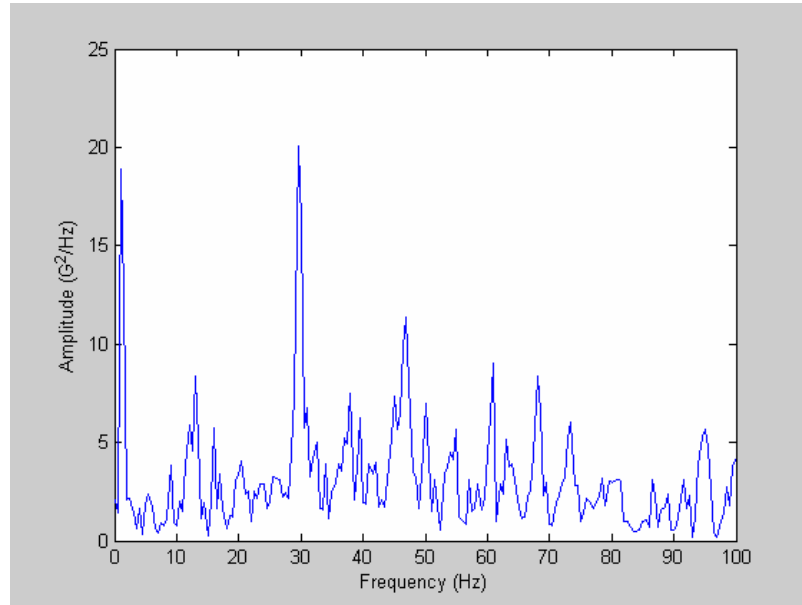
2. FRF measured at point 2:
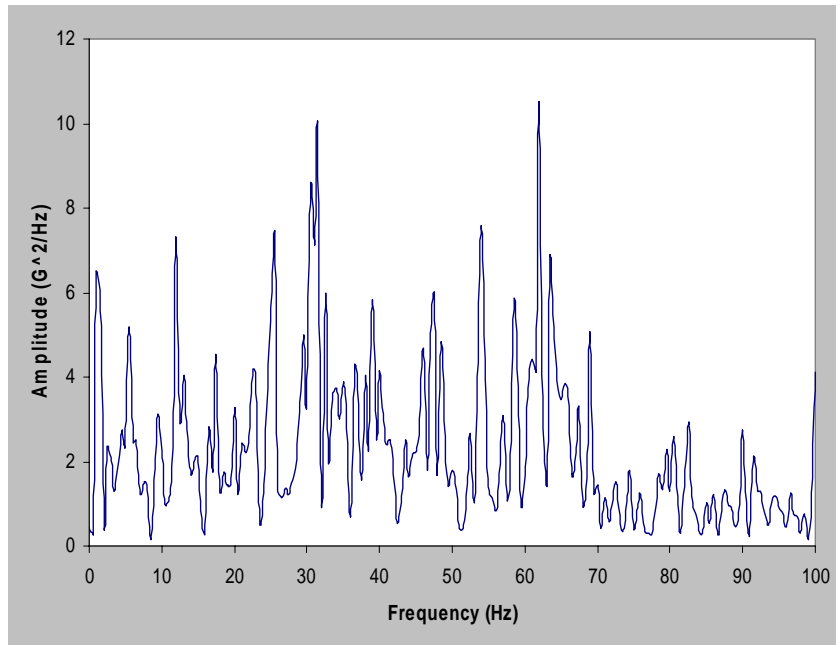
3. FRF measured at point 3:
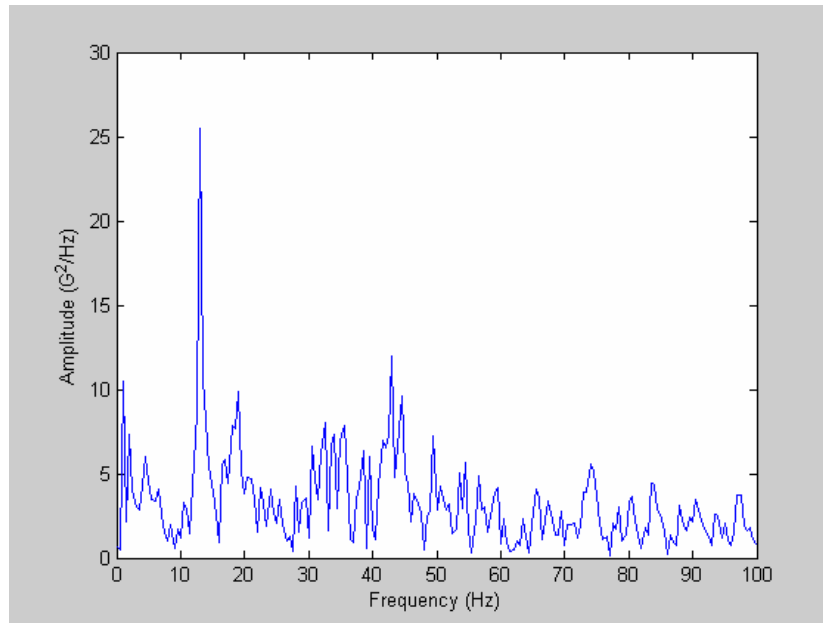
4. FRF measured at point 4:
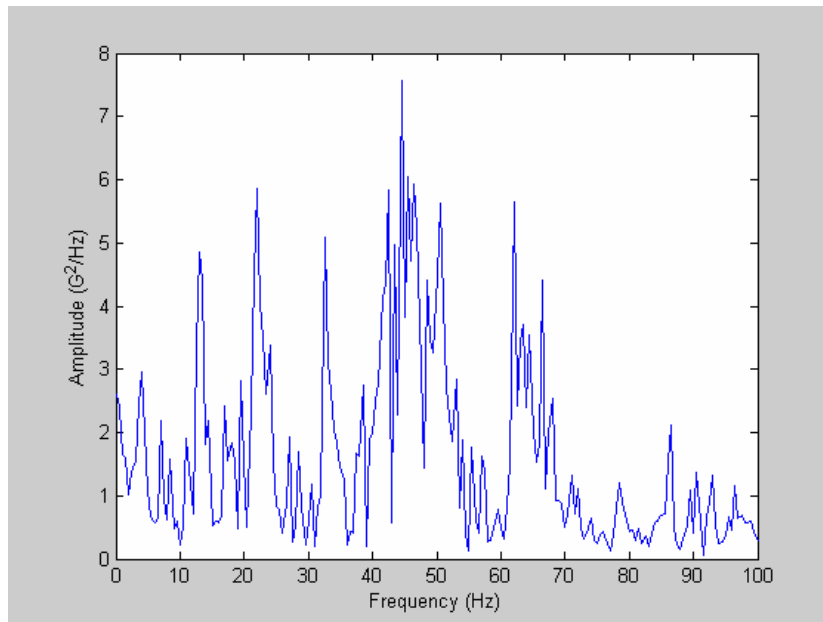
5. FRF measured at point 5:
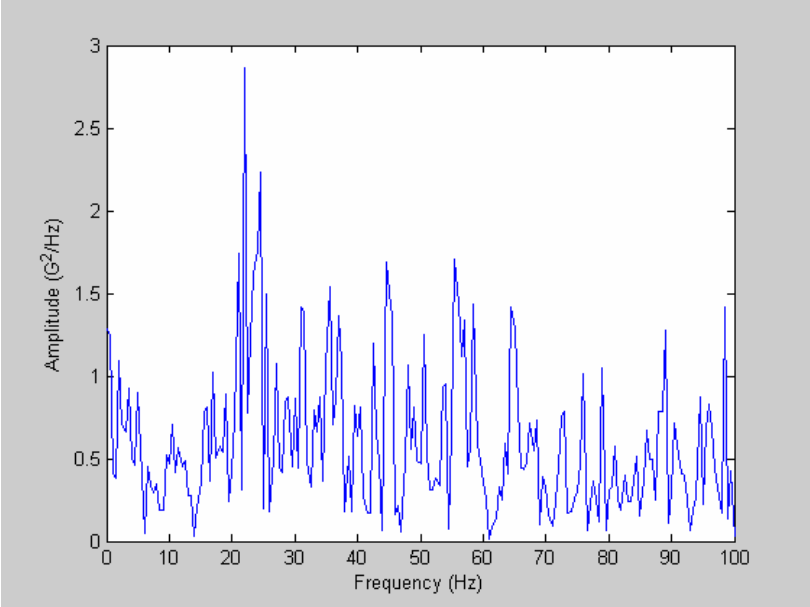
6. FRF measured at point 6
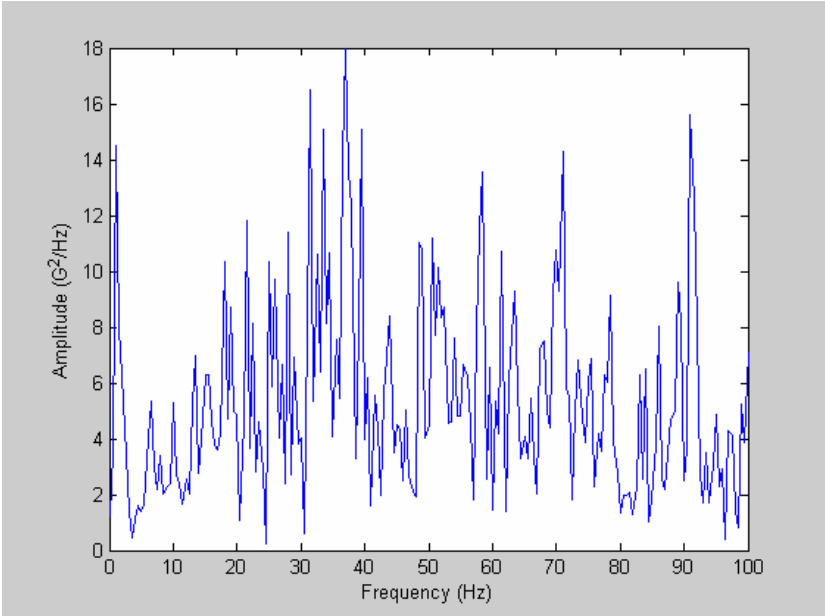
7. FRF measured at point 7:
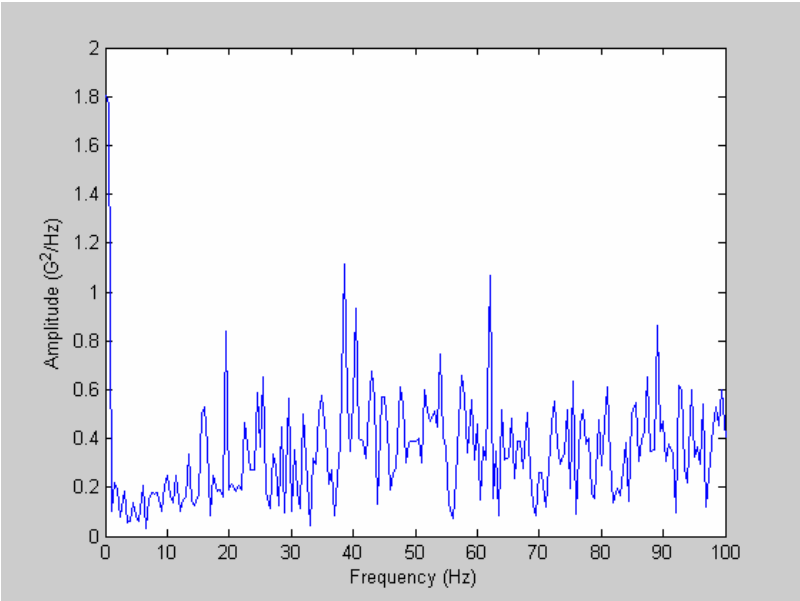
8. FRF measured at point 9 (FRF for point 8 not available):
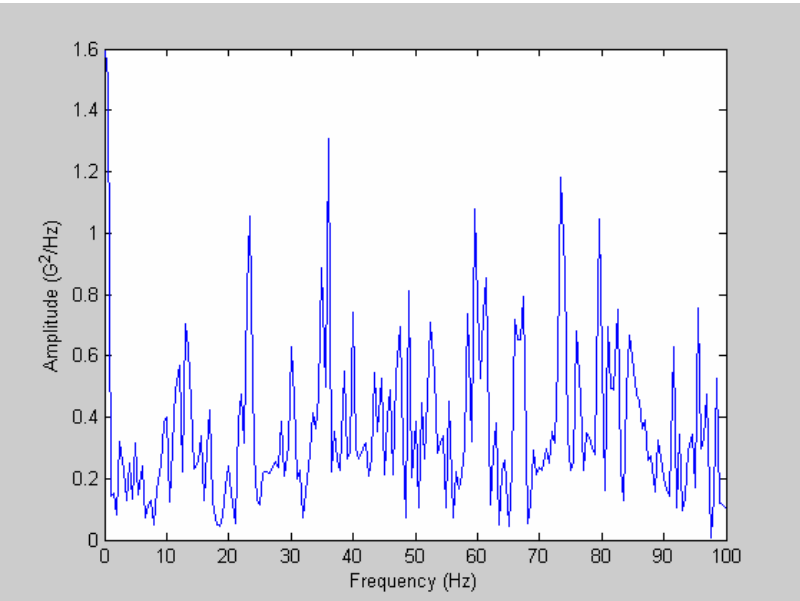
9. FRF measured at point 10:
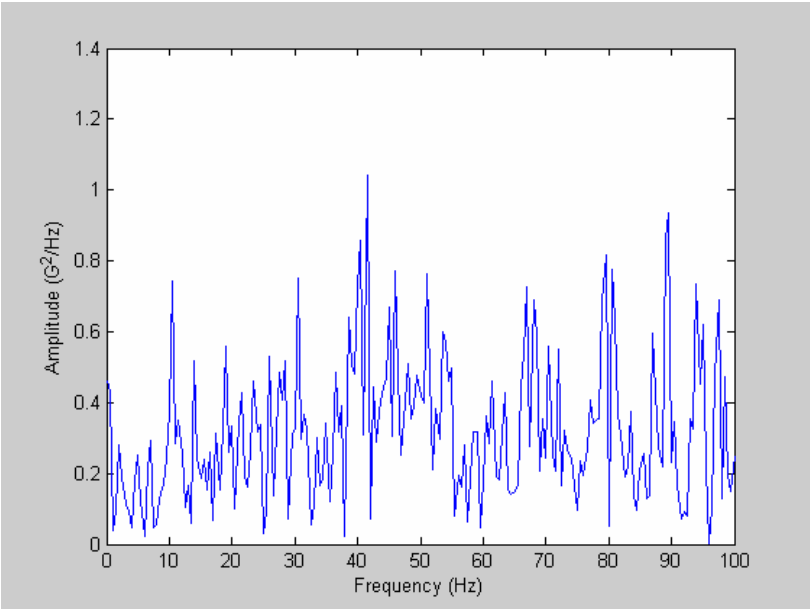
10. FRF measured at point 12 (FRF for point 11 not available):

71
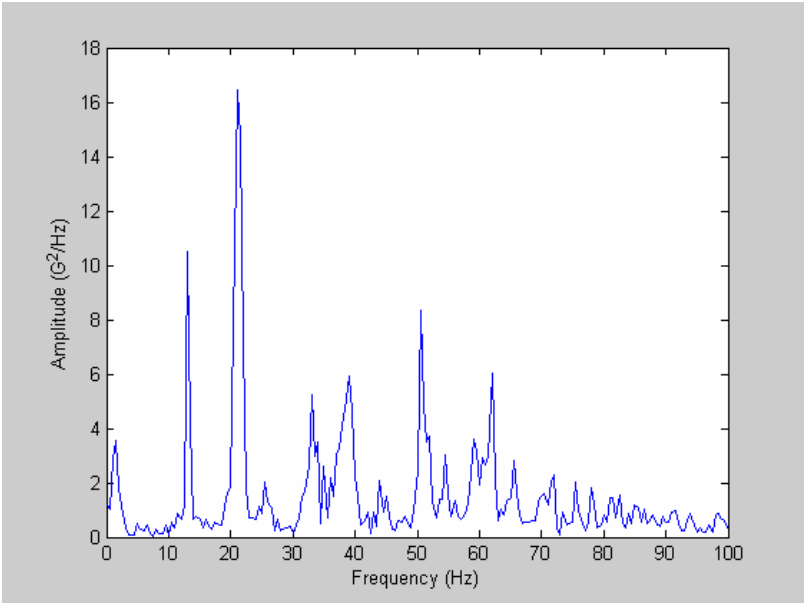
11. FRF measured at point 13:
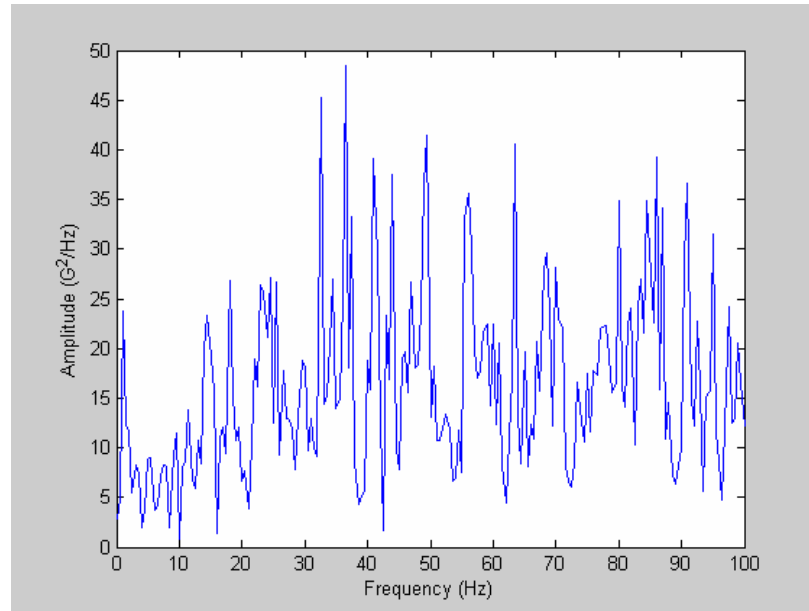
12. FRF measured at point 14:
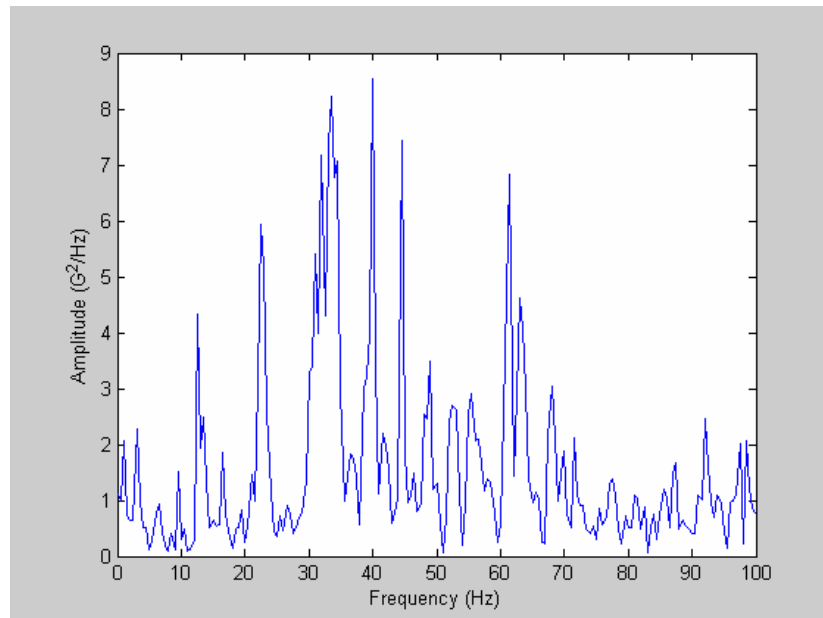
13. FRF measured at point 15:
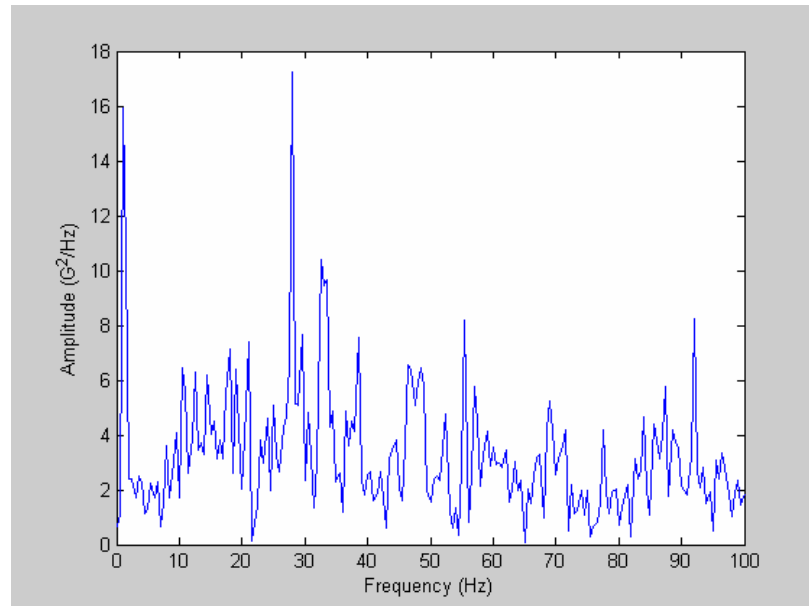
Note: FRFs for points 16 – 24 not available.

APPENDIX 8

1. Mode shape 1 from modal analysis
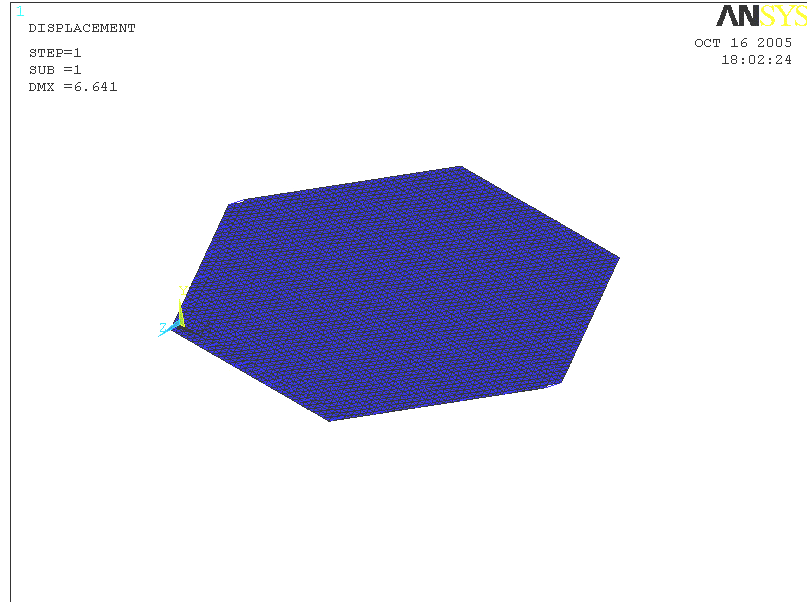
2. Mode 2:
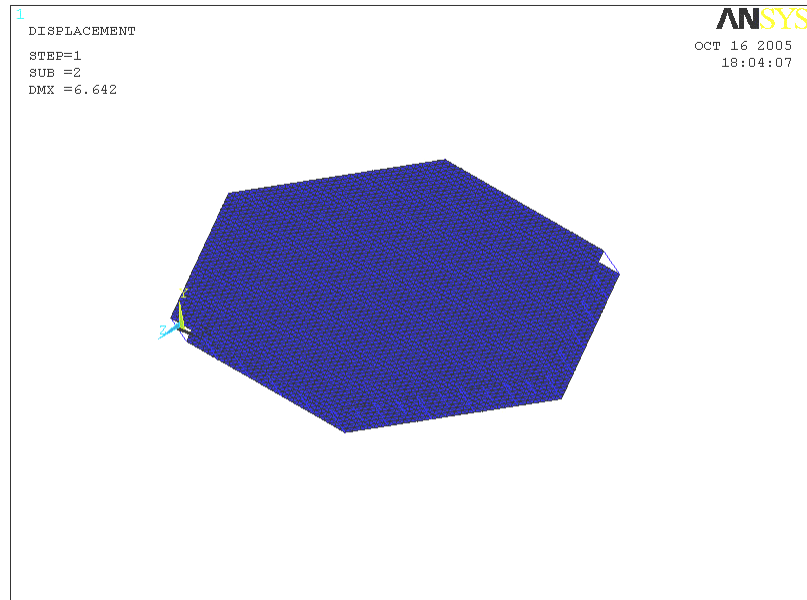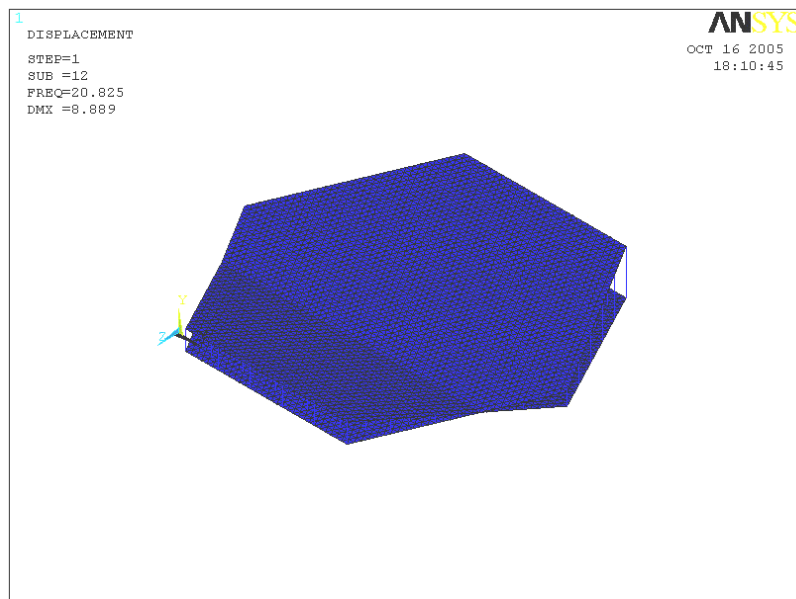
3. Mode 3:
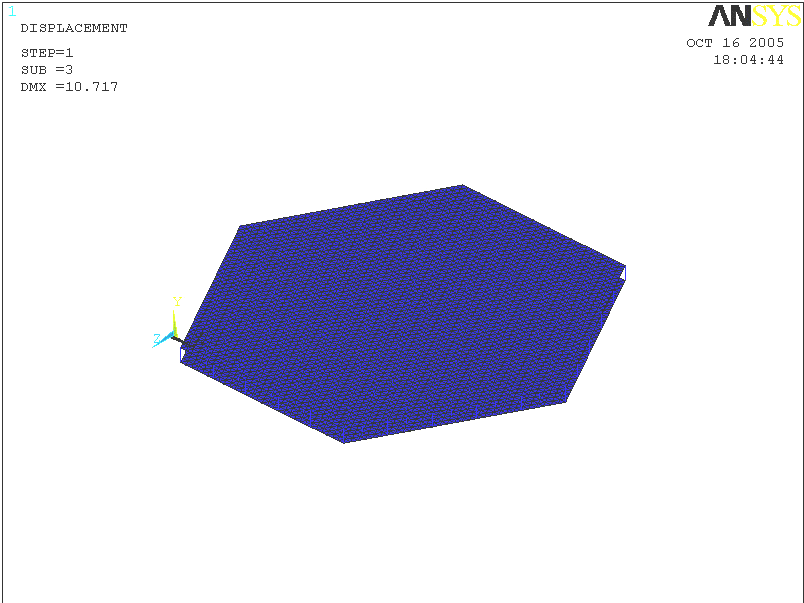
4. Mode 4:
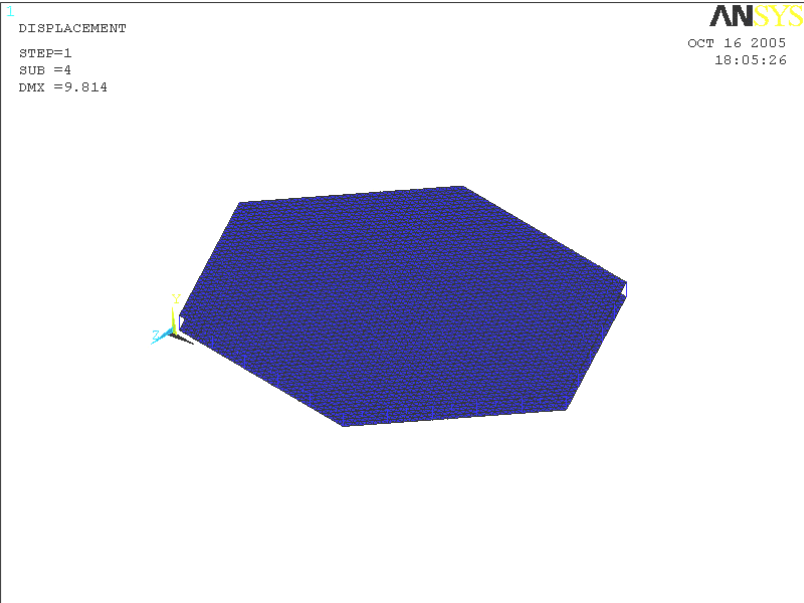
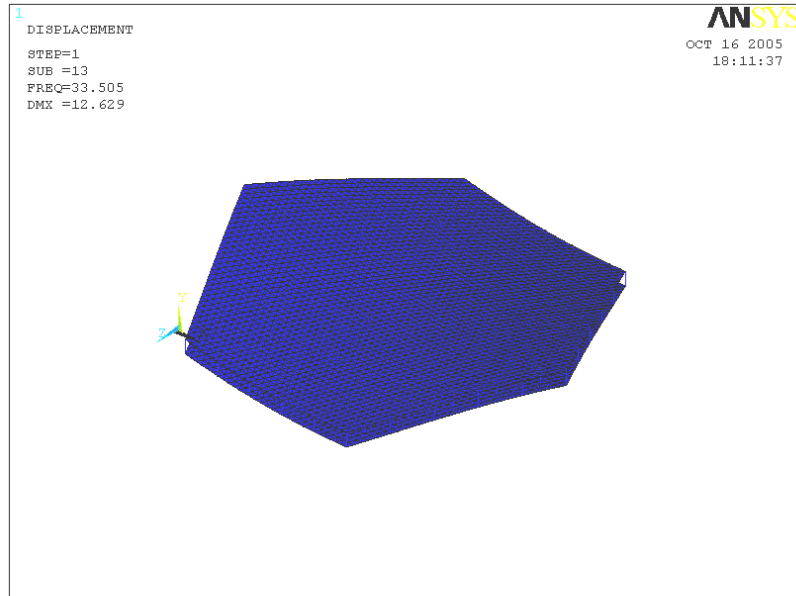5. Mode 5:
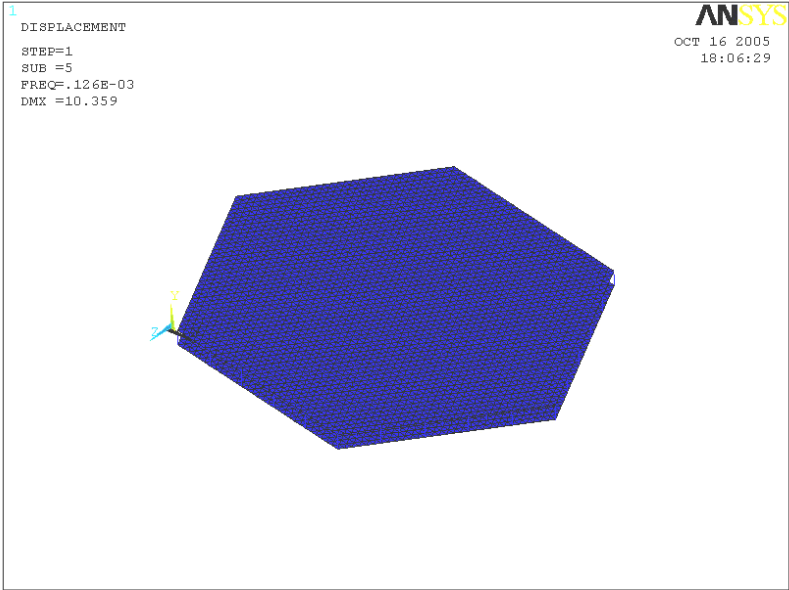
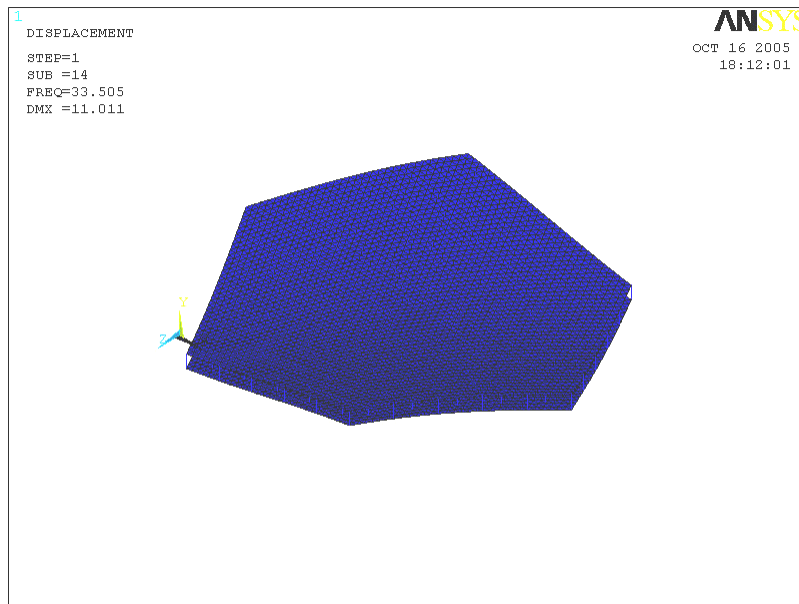6. Mode 6:
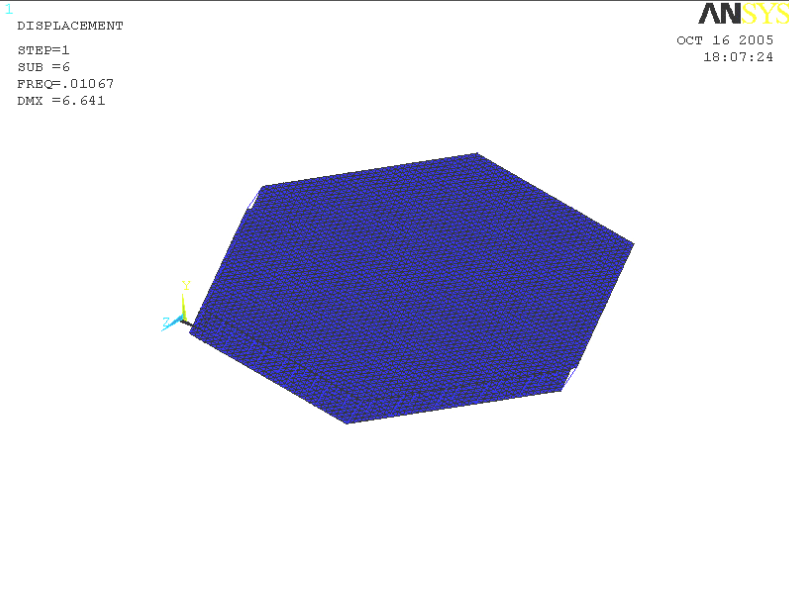
7. Mode 7:
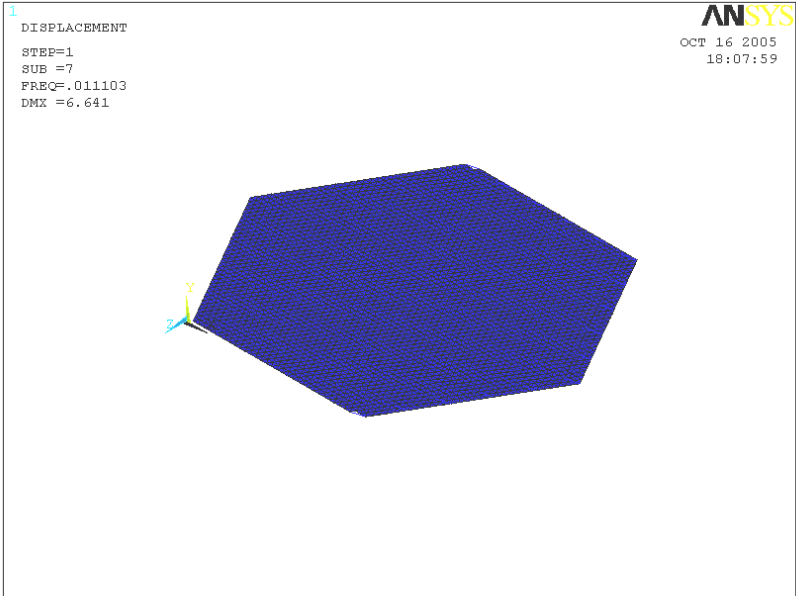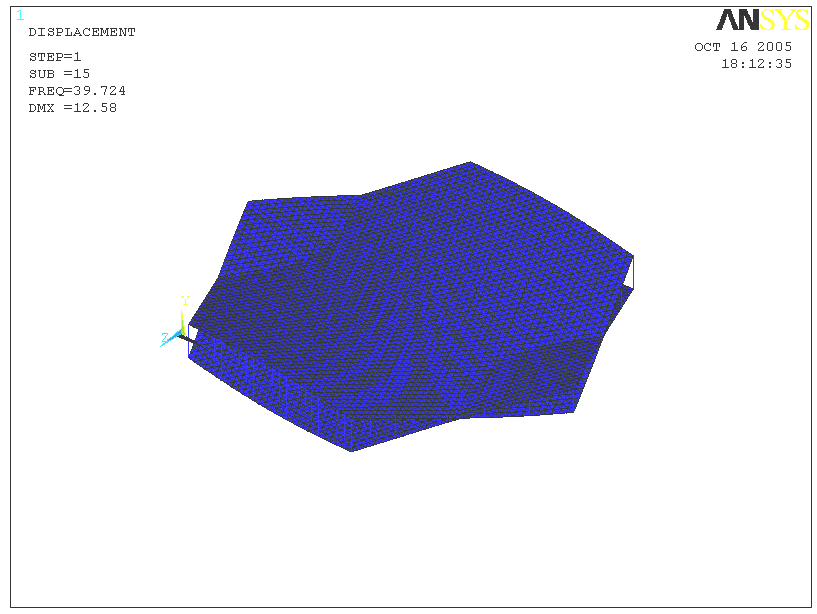

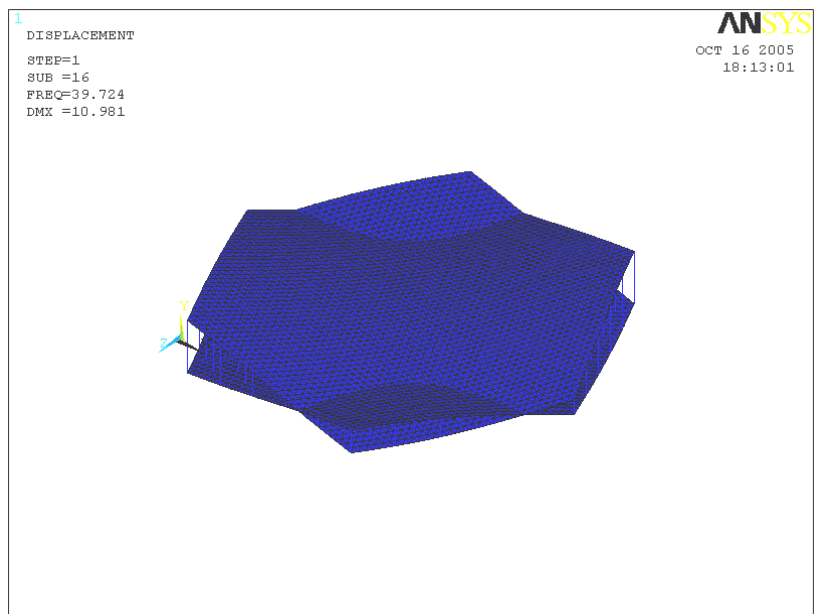8. Mode 8:
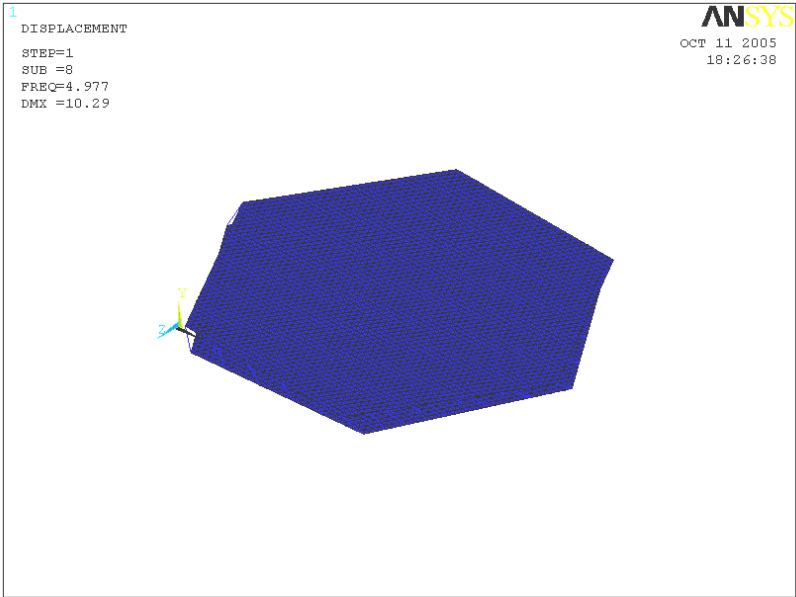
9. Mode 9:
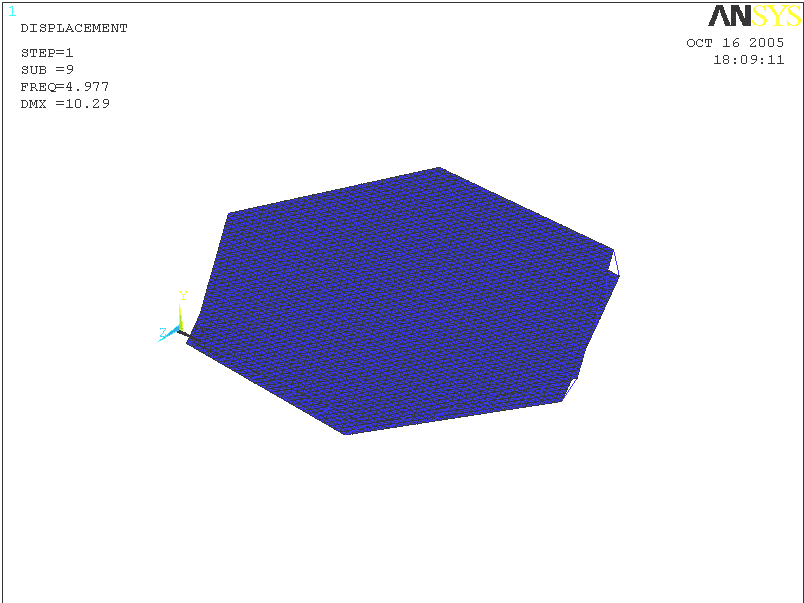
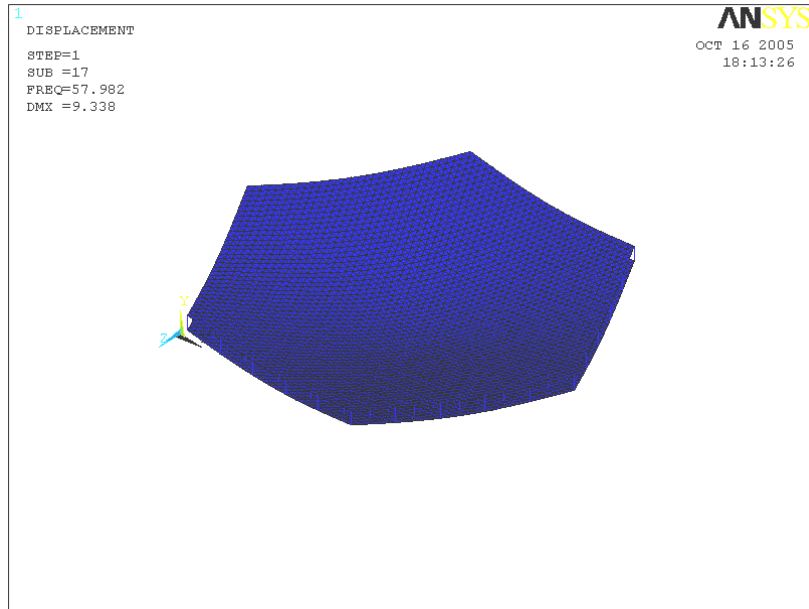10. Mode 10:
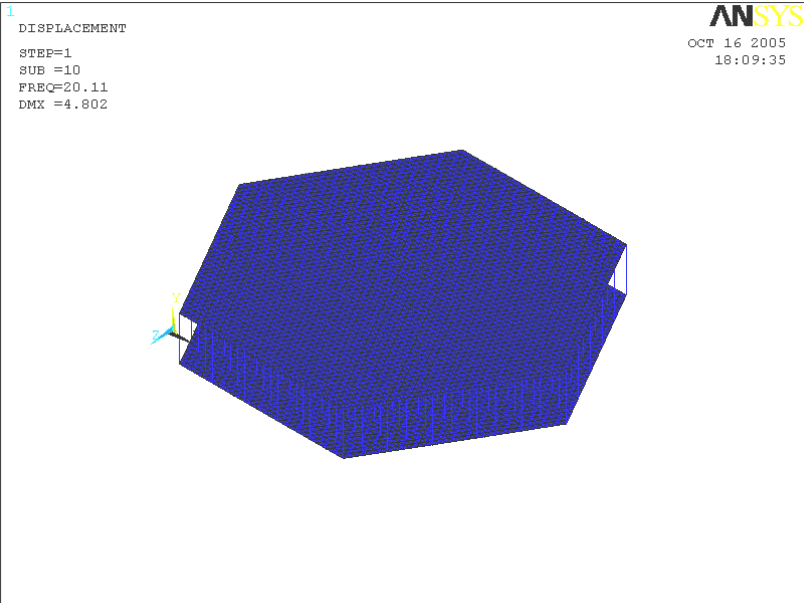
11. Mode 11:
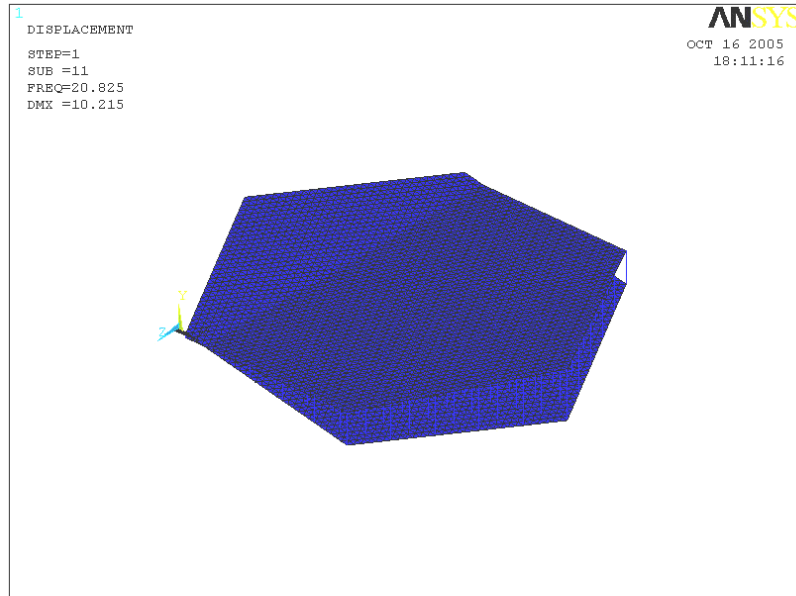
12. Mode 12:

13. Mode 13:

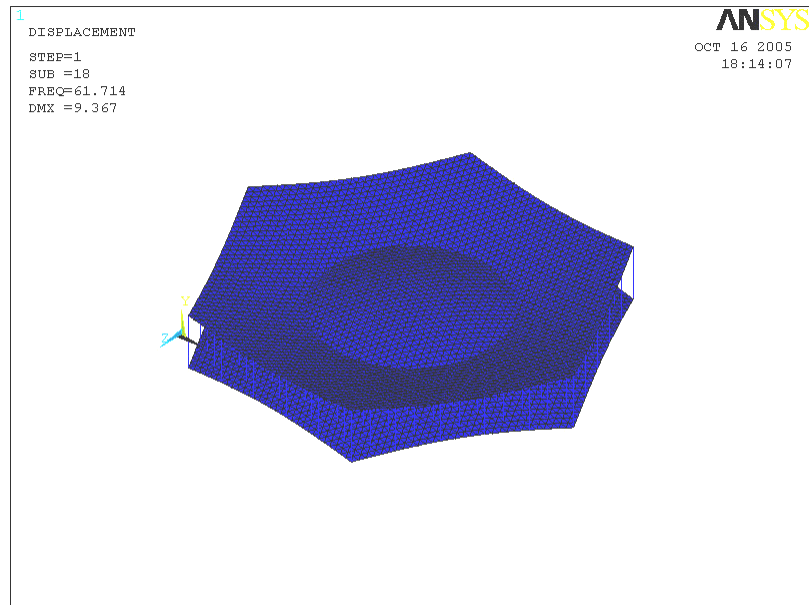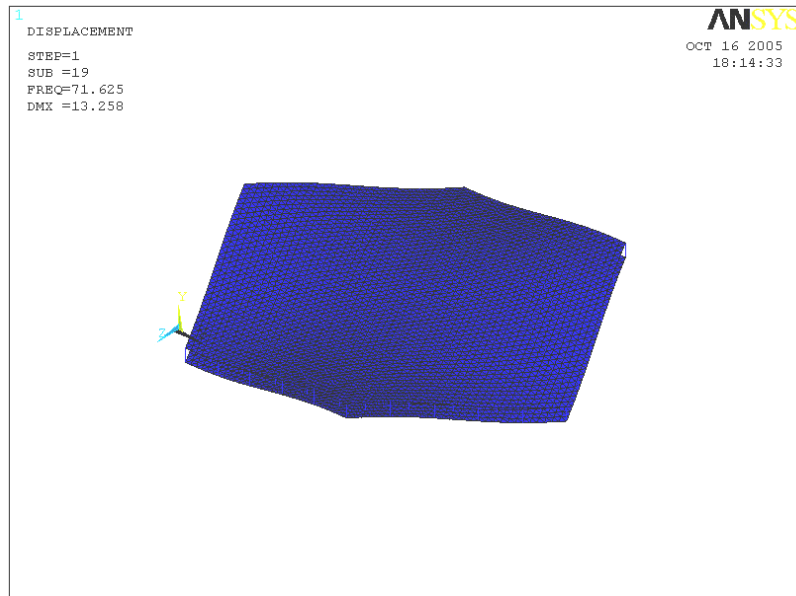14. Mode 14:

15. Mode 15:

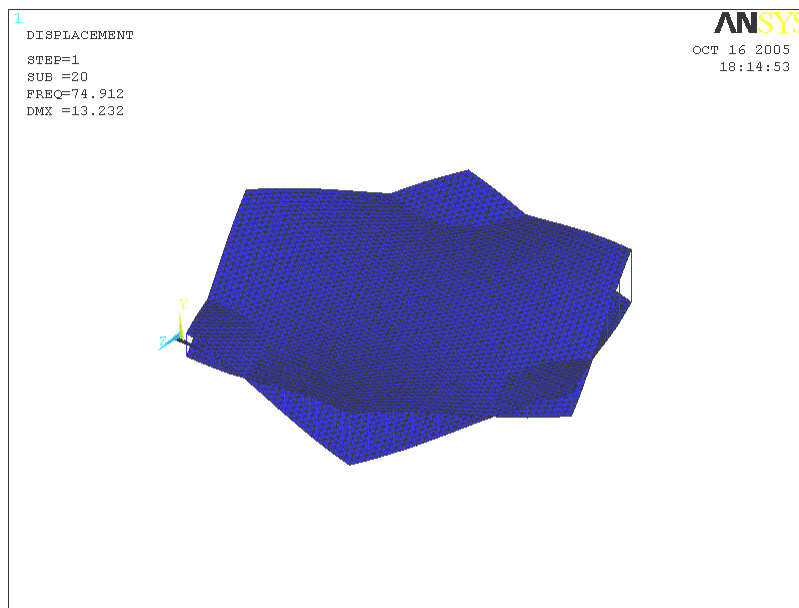16. Mode 16:

17. Mode 17:

18. Mode 18:

19. Mode 19:

20. Mode 20:

REFERENCES

[1] Gossamer Spacecraft: Membrane and Inflatable Structures Technology for Space Application, published by American Institute of Aeronautics and Astronautics (AIAA) in 2001

[2] The proceedings of the 1st Gossamer Spacecraft forum

[3] The proceedings of the 2nd Gossamer Spacecraft forum

[4] The proceedings of the 5th Gossamer Spacecraft forum

[4] http://www.ilcdover.com/products/aerospace_defense/spaceinflatables.htm

[5] http://www.lgarde.com/programs/ird.html

[6] http://www.swales.com/contract/spacetech_rd/sld051.html

[7] http://www.srs.com/srsweb/

[8] http://www.stg.srs.com/

[9] Freeland, R.E., "Significance of the Inflatable Antenna Experiment Technology," AIAA paper: AIAA-98-2104, pp. 2789-2796

[10] Covault. C, "USAF Shifts Technology for New Future in Space," Aviation Week & Space Technology, pp. 44-47, August 17, 1998

[11] Bernasconi. M. C. and Zurbuchen. T, "Lobed Solar Sails for a Small Mission to the Asteroids," Acta Astronautica, Volume 35, pp. 645, 1995

[12] Lester. D. M. and Cannon. D. M, "Foam Inflated Rigidized Truss Structure developed for an SRS Technologies Solar Concentrator," Proceedings of 1996 International Solar Energy Conference, San Antonio, TX, March 31-April 1996, pp. 451-458.

[13] Dornheim. M. A., "Inflatable Structures Taking to Flight," Aviation Week & Space Technology, pp. 60-62, January 25, 1999.

[14] D. J. Ewins, "Modal Testing: Theory and Practice," ISBN 0 86380 017 3.

[15] Kenneth G. McConnell, "Vibration Testing – Theory and Practice," ISBN 0 471 30435 2.

[16] Daniel Todd Griffith, "Experimental and Analytical Modal Analysis of an Inflated Thin Film Torus".

[17] Richard S. Pappa, John O. Lassiter, and Brian P. Ross, 'Structural Dynamics Experimental Activities in Ultra-Lightweight and Inflatable Space Structures", NASA/TM-2001-210857

[18] Kara N. Slade, John O. Lassiter, "Dynamics of an Inflatable Structure in Vacuum and Ambient Conditions", AIAA Journal, Vol. 39, No. 5, May 2001.

[19] Eric Ruggiero and Daniel J. Inman, "Smart Materials in Inflatable Structure Applications", AIAA Paper: AIAA 2002-1563.

[20] Hendry A. Sodano and Daniel J. Inman, "Vibration Testing and Control of an Inflatable Torus Using Multiple Sensors/Actuators", AIAA Paper: AIAA 2003-1644.

[21] Suzanne W. Smith, "Larger Inflatable Self-Rigidizing Polymer Film Structures," final report for contract project submitted to United Applied Technologies.

[22] Jonathan T. Black, "Photogrammetry and Videogrammetry Methods Development for Solar Sails".

[23] Phani Krishnan Thota, "Pattern Evaluation for In-plane Displacement of Thin Films," Masters Thesis work submitted at University of Kentucky, 2003.

[24] Kin Fai Lore, "Efficient Computation of Dynamic Response of Large Inflatable Structures," Masters Thesis, University of Kentucky, 2004.

[25] Arthur L. Palisoc and Yuli Huang, 'Design tool for inflatable space structures," AIM-974 378.

[26] L. Herbeck, M. Eiden, M. Leipold, C. Sickinger, W. Unckenbold, "Development and Testing of Deployable Ultra-Lightweight CFRP-Booms for a Solar Sail," Proceedings of European Conference on Spacecraft Structures, November 2000.

[27] Michael Lou and Houfer Fang, "A Combined Analytical and Experimental Study on Space Inflatable Booms," Aerospace Conference Proceedings, 2000 IEEE.

[28] Lawrie Virgin, "Nonlinear Analysis of Slender Booms for Solar Sails," Duke University, Durham, NC.

Prathik Navalpakkam

Date of Birth: October 23, 1978

Place of Birth: Madurai, India

Work experience:

Fleetwood Enterprises Incorporated

Period: Aug 2004 – Present

Title: Engineer – Recreational Vehicle Group

University of Kentucky, Mechanical Engineering Department

Period: July 2003 –Jul 2004

Title: Research Assistant

University of Kentucky, Mechanical Engineering Department

Period: Aug 2002 – June 2003

Title: Teaching Assistant

Caterpillar India Private Limited, India

Period: Aug 1999 – June 2002

Title: Quality Engineer

Education:

Bachelor of Engineering in Mechanical Engineering, 1999

Bharadhidasan University, Tiruchirapalli, Tamil Nadu, India

Professional Affiliations:

July 2003 – July 2004 Society of Automotive Engineering (SAE) Student Member
Sep 2000 – May 2002 Society of Automotive Engineering Board Member